

GAS MOTION STUDY OF LY α EMITTERS AT $Z \sim 2$
USING FUV AND OPTICAL SPECTRAL LINES^{† ‡}TAKUYA HASHIMOTO¹, MASAMI OUCHI^{2,3}, KAZUHIRO SHIMASAKU^{1,4}, YOSHIAKI ONO²,
KIMIHIKO NAKAJIMA^{1,3}, MICHAEL RAUCH⁵, JANICE LEE^{5,6,7}, AND SADANORI OKAMURA⁸*Accepted for publication in ApJ, 2013 Jan 9*

ABSTRACT

We present the results of Magellan/MMIRS and Keck/NIRSPEC spectroscopy for five Ly α emitters (LAEs) at $z \simeq 2.2$ for which high-resolution FUV spectra from Magellan/MagE are available. We detect nebular emission lines including H α on the individual basis and low-ionization interstellar (LIS) absorption lines in a stacked FUV spectrum, and measure average offset velocities of the Ly α line, $\Delta v_{\text{Ly}\alpha}$, and LIS absorption lines, Δv_{abs} , with respect to the systemic velocity defined by the nebular lines. For a sample of eight $z \sim 2-3$ LAEs without AGN from our study and the literature, we obtain $\Delta v_{\text{Ly}\alpha} = 175 \pm 35 \text{ km s}^{-1}$, which is significantly smaller than that of Lyman-break Galaxies (LBGs), $\Delta v_{\text{Ly}\alpha} \simeq 400 \text{ km s}^{-1}$. The stacked FUV spectrum gives $\Delta v_{\text{abs}} = -179 \pm 73 \text{ km s}^{-1}$, comparable to that of LBGs. These positive $\Delta v_{\text{Ly}\alpha}$ and negative Δv_{abs} suggest that LAEs also have outflows. In contrast to LBGs, however, the LAEs' $\Delta v_{\text{Ly}\alpha}$ is as small as $|\Delta v_{\text{abs}}|$, suggesting low neutral hydrogen column densities. Such a low column density with a small number of resonant scattering may cause the observed strong Ly α emission of LAEs. We find an anti-correlation between Ly α equivalent width (EW) and $\Delta v_{\text{Ly}\alpha}$ in a compilation of LAE and LBG samples. Although its physical origin is not clear, this anti-correlation result appears to challenge the hypothesis that a strong outflow, by means of a reduced number of resonant scattering, produces a large EW. If LAEs at $z > 6$ have similarly small $\Delta v_{\text{Ly}\alpha}$ values, constraints on the reionization history derived from the Ly α transmissivity may need to be revised.

Subject headings: cosmology: observations — galaxies: formation — galaxies: evolution — galaxies: high-redshift —

1. INTRODUCTION

Ly α emitters (LAEs) are objects with a large rest-frame Ly α equivalent width, $\text{EW}(\text{Ly}\alpha) \gtrsim 20-30 \text{ \AA}$. This population is usually selected using a narrow band filter for Ly α emission combined with a broad band filter which measures continuum emission around Ly α . Very recently, nearby LAEs down to $z \sim 0.2$ have also been studied with GALEX data (e.g., Cowie et al. 2011). Previous studies have revealed that most (high- z) LAEs are young,

low-mass galaxies with small dust extinction, while some are old, massive, and dusty (Ono et al. 2010a). Morphological studies have revealed that LAEs are smaller than typical high- z star forming galaxies (Bond et al. 2009, 2010). Thus, LAEs are among the building block candidates in the Λ Cold Dark Matter (CDM) model, where smaller and less massive galaxies merge to be larger and massive ones (Rauch et al. 2008).

Gas exchanges between galaxies and the ambient intergalactic medium (IGM), i.e., outflows and inflows, are thought to play important roles in galaxy evolution. Outflows are driven by supernovae (SNe), stellar winds from massive stars, and AGN activity (Heckman et al. 1990; Murray et al. 2005; Choi & Nagamine 2011). Galaxies which lost cold gas via outflows may experience a reduction or even termination of subsequent star formation. In contrast, cold gas supplied by inflows may increase the star formation, especially when they comes in the form of dense, filamentary gas streams ('cold accretion'; e.g. Dekel et al. 2009). Gas exchanges will also affect the chemical evolution of galaxies and the IGM, and thus have played important roles in establishing the mass-metallicity relation across cosmic time (e.g., Larson 1974; Tremonti et al. 2004; Erb et al. 2006a).

Outflows have been found in nearby starburst galaxies (Heckman et al. 1990), nearby ULIRGs (Martin 2005), Lyman-break galaxies (LBGs) at $z \sim 2-3$ (Pettini et al. 2002; Shapley et al. 2003), and BX/BM galaxies at $z \sim 2$ (Steidel et al. 2010). These studies have made use of the fact that FUV low-ionization interstellar (LIS) absorption lines, which are generated when continuum photons encounter the outflowing gas, are blue-shifted with re-

thashimoto_at_astron.s.u-tokyo.ac.jp

¹ Department of Astronomy, Graduate School of Science, The University of Tokyo, Tokyo 113-0033, Japan² Institute for Cosmic Ray Research, The University of Tokyo, 5-1-5 Kashiwanoha, Kashiwa, Chiba 277-8582, Japan³ Kavli Institute for the Physics and Mathematics of the Universe, The University of Tokyo, 5-1-5 Kashiwanoha, Kashiwa, Chiba 277-8583, Japan⁴ Research Center for the Early Universe, Graduate School of Science, The University of Tokyo, Tokyo 113-0033, Japan⁵ Observatories of the Carnegie Institution of Washington, 813 Santa Barbara Street, Pasadena, CA 91101, USA⁶ Space Telescope Science Institute, Baltimore, MD, USA⁷ Carnegie Fellow⁸ Department of Advanced Sciences, Faculty of Science and Engineering, Hosei University, 3-7-2 Kajino-cho, Koganei-shi, Tokyo 184-8584, Japan[†] Some of the data presented herein were obtained at the W. M. Keck Observatory, which is operated as a scientific partnership among the California Institute of Technology, the University of California, and the National Aeronautics and Space Administration. The Observatory was made possible by the generous financial support of the W. M. Keck Foundation.[‡] Based in part on data collected at the Subaru Telescope, which is operated by the National Astronomical Observatory of Japan.

spect to the systemic redshift measured by nebular emission lines such as H α originated from HII regions in the galaxy.

Examining the incidence of outflows in LAEs is of interest, because LAEs are generally less massive ($\lesssim 10^9 M_\odot$; Nilsson et al. 2007; Finkelstein et al. 2008; Ono et al. 2010a,b; Nakajima et al. 2012a) than, e.g., LBGs (10^{10} – $10^{11} M_\odot$; Shapley et al. 2004; Erb et al. 2006b) and BzK-selected galaxies (10^{10} – $10^{11} M_\odot$; e.g., Daddi et al. 2004; Yuma et al. 2012), and thus have shallower gravitational potentials. Some authors have argued the importance of outflows from less massive galaxies in chemical enrichment (e.g., Larson 1974). However, FUV continua of LAEs are too faint for LIS absorption lines to be reliably measured with current facilities.

Ly α is also used to probe the gas kinematics. The Ly α line is known to have complex profiles caused by its resonant nature. Many theoretical and observational studies have shown that outflowing gas leads to a redshifted Ly α line with respect to the systemic redshift (e.g., Verhamme et al. 2006; Steidel et al. 2010), giving a positive Ly α offset velocity, $\Delta v_{\text{Ly}\alpha}$. In the case of an outflow, back-scattered (i.e., redshifted) Ly α photons have more chance of escape because they drop out of resonance with the foreground gas. However, it is very difficult to obtain high-resolution nebular emission spectra for LAEs because they are faint compared to strong sky emission.

Prior to our study, only four LAEs have both high-resolution Ly α and nebular line spectra: two from McLinden et al. (2011) and two from Finkelstein et al. (2011). McLinden et al.’s objects have $\Delta v_{\text{Ly}\alpha} = 125 \pm 17.3$ and 342 ± 18.3 km s $^{-1}$, respectively, and Finkelstein et al.’s objects have $\Delta v_{\text{Ly}\alpha} = 288 \pm 37$ (photometric) ± 42 (systematic) and $189 \pm 35 \pm 18$ km s $^{-1}$, respectively (see also Chonis et al., in preparation). The fact that all four have $\Delta v_{\text{Ly}\alpha} > 0$ suggests that outflows are common in LAEs, but due to the small sample sizes obtained so far, there has not been a statistical discussion of the gas motions of LAEs.

Answering the fundamental question as to why LAEs have strong Ly α emission is crucial for understanding the physical nature of LAEs. Some studies have shown that outflows facilitate the escape of Ly α photons from galaxies (e.g., Kunth et al. 1998) as they reduce the number of resonant scattering. Indeed, Verhamme et al. (2006, 2008) have carried out Ly α radiative transfer simulations, and claimed that expanding shell models can account for observed Ly α spectral profiles of LBGs. However, while certain aspects of the Ly α radiative transfer mechanism of high- z galaxies can be understood in the context of outflows, the reason for the strong Ly α emission of LAEs is still an open question.

In order to address these questions, we are conducting near infrared spectroscopy for optically confirmed LAEs at $z \simeq 2.2$ promising for detecting nebular emission lines. High-resolution spectra of nebular emission lines are essential for measuring the offset velocities of the Ly α line, $\Delta v_{\text{Ly}\alpha}$, and of LIS absorption lines, Δv_{abs} , with respect to the systemic velocity. The redshift of $z \simeq 2.2$ is favored since we can simultaneously observe Ly α , LIS absorption lines (e.g., [SiII]), [OI], and [CII]), and optical nebular lines (e.g., [OII], H β , [OIII], and H α) from the ground. Furthermore, we can compare the kin-

ematics and Ly α radiative transfer of LAEs with those of brighter and more massive galaxies at similar redshifts, e.g., LBGs, obtained by previous studies.

We successfully detect for several LAEs nebular emission lines on the individual basis and LIS absorption lines in a stacked FUV spectrum, to measure $\Delta v_{\text{Ly}\alpha}$ and Δv_{abs} . We also derive physical quantities such as EW(Ly α), Ly α escape fraction ($f_{\text{esc}}^{\text{Ly}\alpha}$), star formation rate (SFR), stellar mass, and the size of the star-forming region from the spectral data and photometric data (SED fitting). Using these quantities, we discuss the gas kinematics of LAEs and give implications on the physical origin of the strong Ly α emission.

This paper is organized as follows. Our near infrared spectroscopy is described in §2. After performing SED fitting in §3, we derive $\Delta v_{\text{Ly}\alpha}$, Δv_{abs} , and several observational quantities for our LAEs in §4. A discussion in the context of outflow and Ly α radiative transfer is given §5, followed by conclusions in §6. Throughout this paper, magnitudes are given in the AB system (Oke & Gunn 1983), and we assume a Λ CDM cosmology with $\Omega_m = 0.3$, $\Omega_\Lambda = 0.7$ and $H_0 = 70$ km s $^{-1}$ Mpc $^{-1}$.

2. SPECTROSCOPIC DATA

2.1. Targets of our NIR Spectroscopy

Our targets for near infrared spectroscopy are selected from samples of $z \simeq 2.2$ LAEs in the COSMOS and the Chandra Deep Field South (hereafter CDFS) constructed by K. Nakajima et al. (in preparation) in the same manner as in Nakajima et al. (2012a). These LAE samples are based on narrow-band (NB387) imaging with Subaru/Suprime-Cam, supplemented by public broadband data. NB387 is our custom-made filter with a central wavelength and FWHM of 3870 Å and 94 Å, respectively (Nakajima et al. 2012a). The LAEs have been selected by imposing the following color criteria:

$$\begin{aligned} u^* - \text{NB387} &> 0.5 \ \& \ B - \text{NB387} > 0.2 \ (\text{COSMOS}) \\ U - \text{NB387} &> 0.8 \ \& \ B - \text{NB387} > 0.2 \ (\text{CDFS}). \end{aligned} \quad (2)$$

The COSMOS (CDFS) sample contains 619 (1,108) LAEs with $\text{EW}_{\text{Ly}\alpha} \gtrsim 30 \text{ Å}$ down to $\text{NB387} = 26.1$ (26.4). Among them, two objects in the CDFS sample (CDFS-3865, CDFS-6482) and three in the COSMOS sample (COSMOS-13636, COSMOS-30679, COSMOS-43982) have a high-quality Magellan/MagE spectrum of Ly α (M. Rauch et al., in preparation). These five objects are our targets of NIR spectroscopy. They have typical NB387 excesses among the whole LAE sample in each field while having relatively bright NB387 magnitudes.

2.2. Near Infrared Spectroscopy

We observed the two CDFS objects on 2010 October 21 with Magellan/MMIRS using the HK grism covering 1.254 – 2.45 μm . The total exposure time was 10800s for each object. The slit width was 0."5 resulting in $R \equiv \lambda/\Delta\lambda \sim 1120$. A two-point dither pattern (A1,B1,A2,B2,A3,B3,...) was adopted. The A0V standard star HIP-16904 was also observed. The sky was clear through our observation run, with seeing sizes of 0."5 – 0."9.

The three COSMOS objects were observed on 2011 February 10 and 11 with Keck-II/NIRSPEC. COSMOS-30679 was observed with NIRSPEC-3 (J band; 1.15 –

1.36 μ m), NIRSPEC-5 (H band; 1.48 – 1.76 μ m), and NIRSPEC-6 (K band; 2.2 – 2.43 μ m) filters in the low-resolution mode, while COSMOS-13636 and COSMOS-43982 were observed with the K band alone. Furthermore, we observed CDFS-3865 with the J band targeting [OII] $\lambda\lambda$ 3726, 3729. Total exposure times are shown in Table 1. The slit width was 0.''76 for all three objects, corresponding to $R \sim 1500$ for all grisms. A two-point dither pattern was adopted. We simultaneously observed reference stars, which we used for blind offsets (see Finkelstein et al. 2011; Yang et al. 2011) because of the faintness of our targets. The A0V standard star HIP-13917 was also observed. The sky was clear in our observing nights, with seeing sizes of 0.''6 – 0.''9. A summary of the spectroscopic observations is given in Table 1.

2.3. Data Reduction

We reduced the MMIRS data using IRAF tasks and the COSMOS package which is the standard reduction pipeline for Magellan/IMACS. The MMIRS detector is read out non-destructively during a single exposure, and individual read-outs are stored as separate extensions in a FITS file through which we know whether and when a particular pixel is saturated. Bias subtraction and flat fielding were processed for each read-out using IRAF `mscred` package to treat data of this format. Then we ran `mmfixen` package which takes advantage of its sampling. This essentially fits a line to different values for a given pixel in each readout, and outputs the slope of this linear fit to the final collapsed image. Wavelength calibration and distortion correction were processed for each frame using the COSMOS package. Although we obtained arc lamp calibration images, we used OH lines for wavelength calibration. We then performed the following operation to remove sky background: $C1 = B1 - (A1 + A2)/2$, $C2 = B2 - (A2 + A3)/2$. After this operation, we ran `subsky` in the COSMOS package¹¹ on each frame to remove residual sky lines. Resultant frames ($C1, C2, \dots$) are then stacked to have a final 2D frame using `sumspec-2d` and `extract-2dspec` in the COSMOS package. 1D spectrum extraction was carried out using `apall` in IRAF. The telluric absorption correction and flux calibration were conducted using the standard star frames. The flux-calibrated 1D spectra of the two objects are shown in Figure 1.

We reduced the NIRSPEC data using mainly IRAF tasks. Details of the reduction procedure is described in Nakajima et al. (2012b). The flux-calibrated 1D spectra of the three objects are shown in Figure 2.

2.4. Emission Line Detections and Measurements

We determine a line to be detected, if there exists an emission line above the 3σ sky noise around the wavelength expected from the Ly α redshift, where sky noise is calculated from the spectrum within 100 Å from the line wavelength. Table 2 summarizes the line detections. For each detected line, we fit a Gaussian function to calculate its central wavelength, FWHM, and flux. The central wavelength is then converted into the vacuum wavelength after correction for the heliocentric motion of the earth¹², and is adopted for the systemic redshift of the

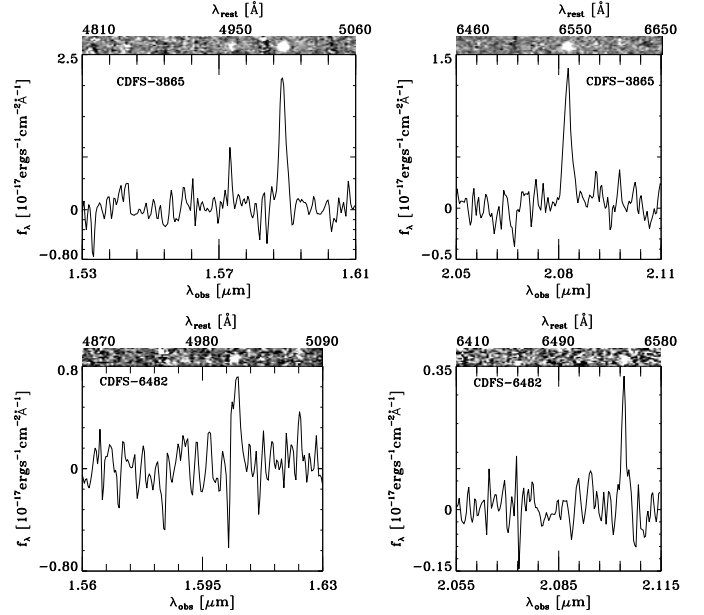


FIG. 1.— Reduced 1D+2D spectra of CDFS-3865 (top) and CDFS-6482 (bottom).

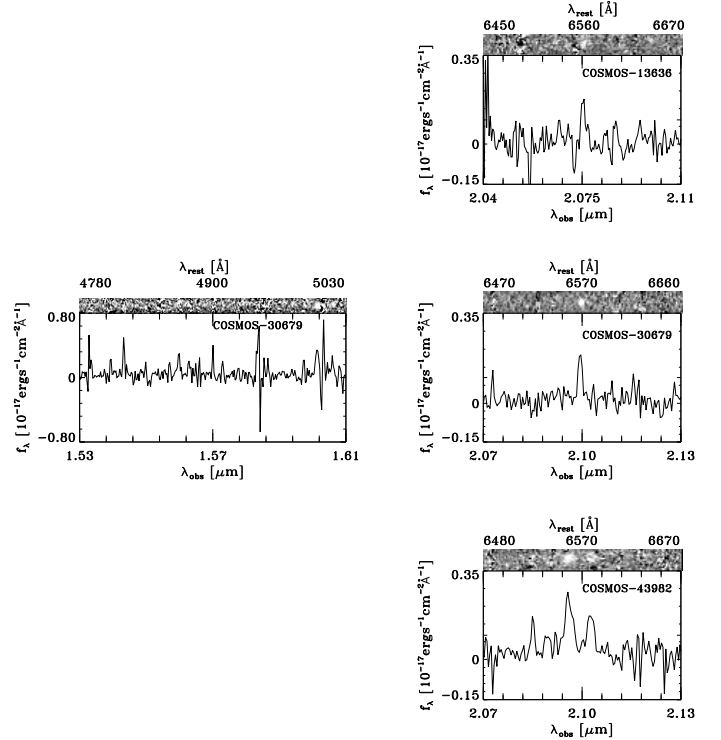


FIG. 2.— Reduced 1D+2D spectra of COSMOS-13636 (top), COSMOS-30679 (middle), and COSMOS-43982 (bottom). H -band data were taken only for COSMOS-30679.

object. For the four objects with multiple line detections, we confirm that the redshifts of the lines agree within 1σ errors, and adopt their weighted mean for the systemic redshift. [OII] is not used in the redshift measurement because the 3726Å/3729Å doublet is not resolved in our spectra. The $H\beta$ line for CDFS-3865 is not used, either, because of the low S/N ratio. We also derive 1σ upper limits of fluxes for all undetected lines. The emission line measurements are summarized in Table 2.

¹¹ This uses the Kelson procedure (cf, Kelson 2003).

¹² <http://fuse.pha.jhu.edu/support/tools/vlsr.html>

TABLE 1
SUMMARY OF OUR OBSERVATIONS

Object	α (J2000)	δ (J2000)	z (Ly α)	L (Ly α) (10^{42} erg s $^{-1}$)	Dates	t_{exp} (s)
(1)	(2)	(3)	(4)	(5)	(6)	(7)
CDFS-3865	03:32:32.31	-28:00:52.20	$2.17507^{+0.00104}_{-0.00004}$	29.8 ± 4.9	2010 Oct 21	5100 (<i>J</i>), 10800 (<i>HK</i>)
CDFS-6482	03:32:49.34	-27:59:52.35	$2.20610^{+0.00049}_{-0.00002}$	15.4 ± 8.1	2010 Oct 21	10800 (<i>HK</i>)
COSMOS-13636	09:59:59.38	+02:08:38.36	2.16229 ± 0.00008	11.3 ± 0.5	2011 Feb 10–11	5400 (<i>K</i>)
COSMOS-30679	10:00:29.81	+02:18:49.00	2.20046 ± 0.00008	8.5 ± 0.7	2011 Feb 10–11	5400 (<i>J</i>), 7200 (<i>H</i>), 6300 (<i>K</i>)
COSMOS-43982	09:59:54.39	+02:26:29.96	2.19396 ± 0.00008	11.0 ± 0.5	2011 Feb 10–11	3600 (<i>K</i>)

Notes. (1) Object ID; (2), (3) Right ascension and declination; (4) Redshift of Ly α emission; (5) Ly α luminosity derived from narrow- and broad-band photometry; (6) Dates of observations; (7) Exposure times for the filters shown in parentheses.

TABLE 2
EMISSION LINE PROPERTIES

Object	Line	λ_{rest} (\AA)	λ_{obs} (\AA)	$\lambda_{\text{corr.}}$ (\AA)	z	S/N	Instrument
(1)	(2)	(3)	(4)	(5)	(6)	(7)	(8)
CDFS-3865	[OII]	3727.00	- ^a	- ^a	- ^a	6.2	NIRSPEC
	H β	4861.33	15418.9 ± 4.0	15418.3	2.17162 ± 0.00083	3.2	MMIRS
	[OIII]	4958.91	15735.8 ± 3.5	15735.1	2.17310 ± 0.00071	5.4	MMIRS
	[OIII]	5006.84	15887.1 ± 1.5	15886.4	2.17294 ± 0.00030	15.3	MMIRS
	H α	6562.85	20825.8 ± 1.7	20824.9	2.17315 ± 0.00026	16.0	MMIRS
	[NII]	6583.45	-	-	-	< 1	MMIRS
CDFS-6482	H β	4861.33	-	-	-	< 1	MMIRS
	[OIII]	4958.91	-	-	-	< 1	MMIRS
	[OIII]	5006.84	16048.3 ± 3.8	16047.63	2.205144 ± 0.00076	8.8	MMIRS
	H α	6562.85	21036.9 ± 1.9	21036.02	2.205317 ± 0.00029	5.5	MMIRS
	[NII]	6583.45	-	-	-	< 1	MMIRS
COSMOS-13636	H α	6562.85	20753.5 ± 1.0	20752.36	2.16210 ± 0.00015	7.1	NIRSPEC
	[NII]	6583.45	-	-	-	< 1	NIRSPEC
COSMOS-30679	[OII]	3727.00	- ^a	- ^a	- ^a	4.0	NIRSPEC
	H β	4861.33	-	-	-	- ^b	NIRSPEC
	[OIII]	4958.91	-	-	-	- ^b	NIRSPEC
	[OIII]	5006.84	16013.8 ± 1.2	16013.62	2.19835 ± 0.00024	10.0	NIRSPEC
	H α	6562.85	20993.7 ± 1.3	20993.48	2.19884 ± 0.00019	11.5	NIRSPEC
	[NII]	6583.45	-	-	-	< 1	NIRSPEC
COSMOS-43982	H α	6562.85	20958.50 ± 1.2	20958.26	2.19347 ± 0.00018	11.4	NIRSPEC
	[NII]	6583.45	21026.20 ± 2.1	21025.96	2.19376 ± 0.00032	7.1	NIRSPEC

NOTE. — The weighted mean redshifts for objects with multiple line detection are 2.17306 ± 0.00019 (CDFS-3865), 2.20530 ± 0.00027 (CDFS-6482), 2.19865 ± 0.00015 (COSMOS-30679), and 2.19354 ± 0.00016 (COSMOS-43982). The symbol “-” indicates no detection. (1) Object ID; (2), (3) Line name and its rest-frame wavelength; (4) Observed wavelength of the line; (5) Wavelength of the line corrected for the LSR motion; (6) Redshift; (7) Signal to noise ratio of the line detection; (8) Instrument.

^a [OII] redshift is not shown because it is not reliably measured.

^b S/N upper limit is not shown because the line is contaminated by a strong OH line.

2.5. Checking the presence of AGNs

We examine whether our objects host an AGN in three ways. First, we compare the sky coordinates of the objects with those in deep archival X-ray and radio catalogues. For CDFS, we refer to the X-ray catalogue given by Luo et al. (2008), whose sensitivity limits are 1.9×10^{-17} and 1.3×10^{-16} ergs cm $^{-2}$ s $^{-1}$ for the 0.5–2.0 and 2–8 keV bands, respectively.¹³ For COSMOS, we use the X-ray catalogue by Elvis et al. (2009), whose sensitivity limits are 1.9×10^{-16} (0.5–2.0 keV band), 7.3×10^{-16} (2–10 keV band), and 5.7×10^{-16} ergs cm $^{-2}$ s $^{-1}$ (0.5–10 keV band). We also refer to the radio catalogue constructed by Schinnerer et al. (2010), whose

sensitivity limits are 10–40 μ Jy/beam.¹⁴ No counterpart for the LAEs is found in any of the catalogues.

Second, we look for three high ionization state lines typical of AGNs, CIV λ 1549, HeII λ 1640, and CIII] λ 1909, in the spectra, and detect none of them.

Finally and most importantly, we apply the BPT diagnostic diagram (Baldwin et al. 1981) to our objects, as shown in Figure 3. The solid curve in Figure 3 shows the boundary between star-forming galaxies and AGNs proposed by Kewley et al. (2001) using photoionization models, while the dotted curve is the boundary empirically defined by SDSS objects (Kauffmann et al. 2003). In both cases, star-forming galaxies fall below the curve.

¹³ CDFS <http://www2.astro.psu.edu/users/niel/cdfs/luo2008-chandra-catalog/paper0801.pdf>, and COSMOS <http://www2.astro.psu.edu/users/niel/cdfs/luo2008-chandra-catalog/paper0801.pdf>.

None of our objects has detections of all four lines necessary for the BPT diagram. Thus, as shown in Figure 3, any object but one logically has a possibility of being in the AGN regime. However, we conclude from the following discussion that all but COSMOS-43982 are star-forming galaxies. CDFS-3865 falls below the curves, indicating this is a starburst galaxy. CDFS-6482 has a relatively high [OIII] / H β value (lower limit), but [NII]/H α is not so high. This high [OIII] / H β ratio may not be due to the presence of AGN but due to a higher gas temperature of the HII regions, as has been pointed out for some high-redshift star-forming galaxies (Erb et al. 2006a). Indeed, there are few local AGNs distributed in the range of $\log([\text{NII}]/\text{H}\alpha) \lesssim -0.5$ (e.g., Figure 3 in Finkelstein et al. 2011).

Finkelstein et al. (2009) have also classified a similar object to ours as a star-forming galaxy (blue triangle in Figure 3). A similar argument is made for COSMOS-13636 and COSMOS-30679 whose [NII]/H α ratios are also modest. In contrast, COSMOS-43982 has a very high [NII]/H α ratio. Because we infer that this object is more likely to be an AGN than a star-forming galaxy, we do not use this object in the following discussion.

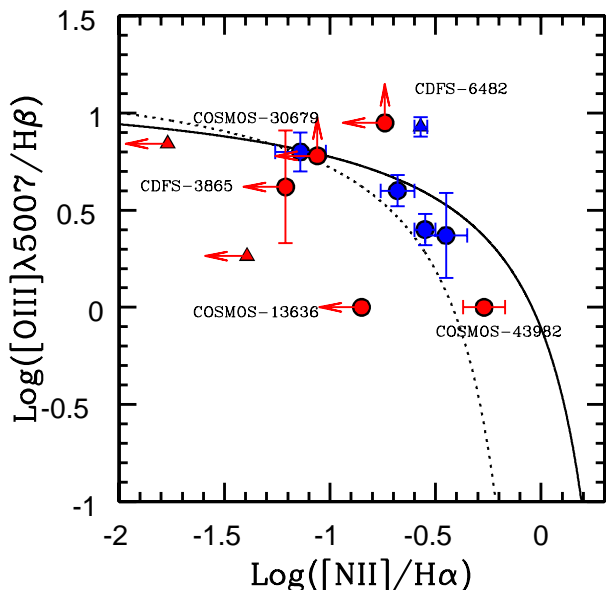


FIG. 3.— BPT diagram. The solid curve represents the boundary between star-forming galaxies and AGNs proposed by Kewley et al. (2001), while the dotted curve is the boundary empirically defined using SDSS objects (Kauffmann et al. 2003). The red circles denote our LAEs. For the purpose of display, COSMOS-13636 and COSMOS-43982, whose [OIII] / H β is not constrained, are placed at $\log([\text{OIII}] / \text{H}\beta) = 0.0$. The red triangles, blue circles, and blue triangle show, respectively, two $z \sim 2.3$ LAEs in Finkelstein et al. (2011), four bins of $z \sim 2.2$ LBGs in Erb et al. (2006a), and a lensed LBG at $z = 2.73$ (Finkelstein et al. 2009).

3. SED FITTING

We perform SED fitting to our objects to derive dust extinction values, SFRs, and stellar masses. The procedure of the SED fitting is the same as that of Ono et al. (2010a). For the CDFS objects, we use 12 bandpasses: B, V, R, I, z, J, H, K data from the MUSYC public data

release¹⁵ (Cardamone et al. 2010), and *Spitzer*/IRAC 3.6, 4.5, 5.8, and 8.0 μm photometry from the *Spitzer* legacy survey of the UDS field. For the COSMOS objects, we use 11 bandpasses: $B, V, r', i',$ and z' data taken with Subaru/Suprime-Cam, J data taken with UKIRT/WFCAM, K_s data taken with CFHT/WIRCAM (McCracken et al. 2010), and *Spitzer*/IRAC 3.6, 4.5, 5.8, and 8.0 μm photometry from the *Spitzer* legacy survey of the UDS field. We use neither u^*/U nor NB387-band data, since the photometry of these bands is contaminated by the IGM absorption and/or Ly α emission. Tables 3 and 4 summarize the broadband photometry of our objects. Basically, the uncertainties in the optical photometry include both photometric errors and systematic errors associated with aperture correction and photometric calibration.

We use the stellar population synthesis model of GALAXEV (Bruzual & Charlot 2003) including nebular emission (Schaerer & de Barros 2009), and adopt a Salpeter initial mass function (Salpeter 1955). Because LAEs are metal poor star-forming galaxies, we choose constant star formation models with a metallicity of $Z/Z_\odot = 0.2$. We use Calzetti's law (Calzetti et al. 2000) for the stellar continuum extinction, $E(B - V)_*$. We apply Madau (1995)'s prescription to correct for the IGM attenuation; at $z \simeq 2.2$, continuum photons shortward of Ly α are absorbed by 18 %. Figure 4 shows the best-fit model spectra with the observed flux densities for individual objects. The physical quantities derived from SED fitting are summarized in Table 5. Because the continuum emission of COSMOS-30679 is blended with a foreground object, we deblend the source with GALFIT (Peng et al. 2002; see Nakajima et al. 2012b for details). While photometry data both before and after deblending are given in Table 4, we use the latter for SED fitting.

4. PHYSICAL QUANTITIES OF OUR LAES

4.1. Velocity Offset Between Ly α and Nebular Lines

We calculate a quantity called the velocity offset of the Ly α line:

$$\Delta v_{\text{Ly}\alpha} = c \frac{z_{\text{Ly}\alpha} - z_{\text{sys}}}{1 + z_{\text{sys}}}, \quad (3)$$

where $z_{\text{Ly}\alpha}$ is the redshift of Ly α emission and z_{sys} is the systemic redshift given in Table 2.

We show the Ly α and H α profiles in Figure 5. Most objects have a Ly α profile which is asymmetric and/or double peaked. Similar to previous studies (Steidel et al. 2010; Yang et al. 2011), we define $z_{\text{Ly}\alpha}$ to be the redshift corresponding to the wavelength at the highest peak. The peak wavelength is determined as follows. First, we roughly constrain the peak position by the eye. For the CDFS objects, we cannot identify where is the highest peak, since the second peak is within the 1σ error in the height of the first peak. In these cases, we regard both as peak candidates and include their wavelength difference as the error in $z_{\text{Ly}\alpha}$ (as listed in Table 1). Then, we fit a Gaussian to the profile only around the peak to derive the peak wavelength, in order to avoid systematic effects due to the asymmetric profile. The Ly α line of COSMOS-30679 is partly contaminated by a cosmic ray. It is, however, unlikely that there is a true peak under

¹⁵ <http://www.astro.yale.edu/MUSYC/>

TABLE 3
BROADBAND PHOTOMETRY OF OUR SAMPLE (CDFS)

Object	<i>B</i>	<i>V</i>	<i>R</i>	<i>I</i>	<i>z</i>	<i>J</i>	<i>H</i>	<i>K</i>	[3.6]	[4.5]	[5.8]	[8.0]
CDFS-3865	23.01 (0.01)	22.94 (0.01)	22.92 (0.01)	23.14 (0.07)	22.93 (0.09)	22.73 (0.18)	22.27 (0.12)	22.38 (0.23)	22.82 (0.05)	22.82 (0.08)	22.51 (0.32)	23.00 (0.56)
CDFS-6482	23.93 (0.02)	23.87 (0.03)	23.78 (0.03)	23.95 (0.14)	23.67 (0.16)	23.50 (0.34)	23.36 (0.31)	23.07 (0.39)	22.88 (0.05)	22.83 (0.08)	23.34 (0.60)	99.99 (-)

NOTE. — All magnitudes are total magnitudes. 99.99 mag indicates a negative flux density. Magnitudes in parentheses are 1σ uncertainties.

TABLE 4
BROADBAND PHOTOMETRY OF OUR SAMPLE (COSMOS)

Object	<i>B</i>	<i>V</i>	<i>r'</i>	<i>i'</i>	<i>z'</i>	<i>J</i>	<i>K_s</i>	[3.6]	[4.5]	[5.8]	[8.0]
COSMOS-13636	24.43 (0.01)	24.21 (0.03)	24.35 (0.03)	24.19 (0.04)	24.24 (0.09)	23.10 (0.34)	23.43 (0.26)	24.10 (0.38)	23.75 (0.53)	99.99 (-)	99.99 (-)
COSMOS-30679 ^a	24.05 (0.01)	23.12 (0.01)	22.91 (0.01)	22.46 (0.01)	22.33 (0.02)	21.15 (0.07)	21.83 (0.07)	22.12 (0.07)	22.57 (0.21)	99.99 (-)	23.06 (2.54)
COSMOS-30679 ^b	24.76 (0.03)	23.82 (0.11)	24.44 (0.28)	24.09 (0.30)	23.49 (0.27)	22.31 (0.27)	23.29 (0.28)	- (-)	- (-)	- (-)	- (-)

NOTE. — All magnitudes are total magnitudes. 99.99 mag indicates a negative flux density. Magnitudes in parentheses are 1σ uncertainties.

^a Before deblending of a foreground source.

^b After deblending of a foreground source.

TABLE 5
RESULTS OF SED FITTING

Object	<i>E(B - V)</i> *	<i>SFR_{SED}</i> ($M_{\odot} \text{ yr}^{-1}$)	<i>M</i> * ($10^9 M_{\odot}$)	χ^2
(1)	(2)	(3)	(4)	(5)
CDFS-3865	$0.185^{+0.009}_{-0.009}$	312^{+41}_{-43}	$3.18^{+0.21}_{-0.13}$	17
CDFS-6482	$0.185^{+0.026}_{-0.018}$	83^{+34}_{-18}	$5.30^{+1.18}_{-0.80}$	5
COSMOS-13636	$0.273^{+0.018}_{-0.079}$	1311^{+17574}_{-1244}	$1.99^{+0.39}_{-1.06}$	21
COSMOS-30679	$0.528^{+0.026}_{-0.026}$	$7510^{+201248}_{-3097}$	$19.75^{+6.53}_{-5.80}$	20

Notes. Stellar metallicity is fixed to $0.2 Z_{\odot}$.
(1) Object ID; (2) Dust extinction; (3) Star formation rate; (4) Stellar mass; (5) χ^2 of the fitting.

the cosmic ray. Even if there is a flux peak just under the cosmic ray, our discussion remains unchanged.

We obtain $\Delta v_{\text{Ly}\alpha} = 190^{+99}_{-18} \text{ km s}^{-1}$ (CDFS-3865), $75^{+52}_{-25} \text{ km s}^{-1}$ (CDFS-6482), $18 \pm 16 \text{ km s}^{-1}$ (COSMOS-13636), and $170 \pm 16 \text{ km s}^{-1}$ (COSMOS-30679). Thus, three out of the four have a positive $\Delta v_{\text{Ly}\alpha}$ beyond the 2σ uncertainty.

There are four LAEs in the literature which have both a Ly α spectrum and a systemic-velocity measurement from a nebular line: two from McLinden et al. (2011) and two from Finkelstein et al. (2011). The $\Delta v_{\text{Ly}\alpha}$ of these four LAEs ranges from ~ 100 to $\sim 300 \text{ km s}^{-1}$, which is similar to our $\Delta v_{\text{Ly}\alpha}$ measurements. We combine these four LAEs with our four to construct a sample of eight LAEs at $z \sim 2 - 3$, and investigate average physical properties of LAEs using them. Figure 6 presents the histogram of $\Delta v_{\text{Ly}\alpha}$ for the eight LAEs. All eight have a positive but relatively small $\Delta v_{\text{Ly}\alpha}$ of up to $\sim 300 \text{ km s}^{-1}$. The average of the eight is $\Delta v_{\text{Ly}\alpha} = 175 \pm 35 \text{ km s}^{-1}$, which is systematically smaller, by $\sim 200 - 300 \text{ km s}^{-1}$, than that of LBGs,

$\Delta v_{\text{Ly}\alpha} \simeq 400 \text{ km s}^{-1}$ (Pettini et al. 2002; Shapley et al. 2003; Steidel et al. 2010; Rakic et al. 2011), at similar redshifts of $z \sim 2 - 3$. There are also two Ly α blobs (LABs; e.g., Steidel et al. 2000; Matsuda et al. 2004; Yang et al. 2009) at $z \sim 2.3$ whose $\Delta v_{\text{Ly}\alpha}$ is measured (Yang et al. 2011). Both have $\Delta v_{\text{Ly}\alpha} = 0 - 200 \text{ km s}^{-1}$ which is comparable with our measurements for LAEs but smaller than those for LBGs.

Figure 7 shows the rest-frame Ly α EW as a function of $\Delta v_{\text{Ly}\alpha}$, where data for LBGs (Reddy et al. 2008; Steidel et al. 2010) and LABs (Yang et al. 2011) are also included in order to cover a wide baseline of EW, $0 - 200 \text{ \AA}$. We fit a linear function to the data points (dotted line in Figure 7), and find an anti-correlation between $\Delta v_{\text{Ly}\alpha}$ and Ly α EW that EW(Ly α) decreases with increasing $\Delta v_{\text{Ly}\alpha}$. It is known that there is an anti-correlation between $\Delta v_{\text{Ly}\alpha} - \Delta v_{\text{abs}}$ and EW(Ly α) in LBGs at $z \sim 3$ (Shapley et al. 2003). However, it should be noted that our finding is different from that, because we measure the velocity offset of Ly α directly from the systemic velocity, while $\Delta v_{\text{Ly}\alpha} - \Delta v_{\text{abs}}$ depends on the kinematics of gas outflows and the Ly α emission mechanism.

4.2. Velocity Offset Between LIS Absorption Lines And Nebular Lines

We examine LIS absorption lines using Magellan/MagE echellette spectrograph data with a medium-high spectral resolution of $R \sim 4100$ (M. Rauch et al., in preparation). We inspect one order of the echelle spectra ranging from 3788 \AA to 4419 \AA in the observed frame. This wavelength range covers Si II $\lambda 1260$, O I $\lambda 1302$, Si II $\lambda 1304$, and C II $\lambda 1335$ lines. These LIS absorption lines are associated with the neutral interstellar medium (ISM: Pettini et al. 2002; Shapley et al. 2003).

Since none of these lines is identified in the individual spectra because of the too faint continua, we make

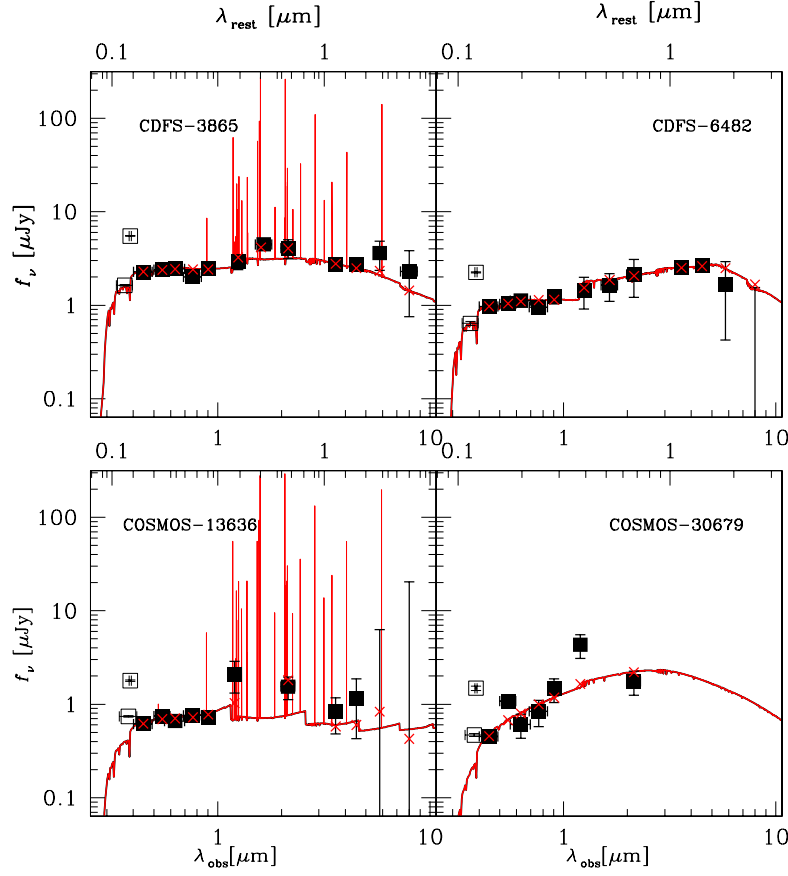


FIG. 4.— Upper (lower) panel shows the SEDs of CDFS (COSMOS) objects. The filled squares denote the photometry points used for SED fitting, while the open squares are those omitted in SED fitting due to the contamination of Ly α emission and IGM absorption. The red lines present the best-fit model spectra, and the red crosses correspond to the flux densities at individual passbands expected from the best-fit models.

a composite spectrum of the four objects as follows. For each object, we shift individual spectral data from the observed to the rest frame using z_{sys} given in Table 2. Then, we stack the spectra of the four objects with statistical weights based on the S/N ratios at 1250–1340 Å.

Figure 8 presents the composite spectrum. An absorption feature is seen near each of the four lines’ wavelengths. For each feature, we fit a Gaussian profile to obtain the rest-frame equivalent width, EW(LIS), and the velocity offset of the line center with respect to the systemic velocity, Δv_{abs} , as summarized in Table 6. We securely detect the Si II $\lambda 1260$ line and the blended O I $\lambda 1302$ + Si II $\lambda 1304$ lines at the 5.2σ and 3.7σ levels, respectively, and marginally detect the C II $\lambda 1335$ line at the 2.0σ level. Note that all lines are blue-shifted with respect to the systemic velocity.

The weighted mean offset velocity of these absorption lines is $\Delta v_{\text{abs}} = -179 \pm 73 \text{ km s}^{-1}$. This value is comparable with those of LBGs, which are typically $\Delta v_{\text{abs}} \sim -150 \text{ km s}^{-1}$ (Shapley et al. 2003; Steidel et al. 2010). Thus, LAEs and LBGs have similar Δv_{abs} values, in contrast to the significant difference in $\Delta v_{\text{Ly}\alpha}$.

4.3. Dust Extinction

TABLE 6
INTERSTELLAR ABSORPTION FEATURES

Ion	λ_{rest} (Å)	f	EW(LIS) (Å)	σ (Å)	Δv_{abs} (km s $^{-1}$)
(1)	(2)	(3)	(4)	(5)	(6)
Si II	1260.4221	1.007	−1.21	0.23	-162 ± 95
O I	1302.1685	0.04887	−1.02 ⁽⁷⁾	0.28 ⁽⁷⁾	$-174 \pm 180^{(7)}$
Si II	1304.3702	0.094	−1.02 ⁽⁷⁾	0.28 ⁽⁷⁾	$-174 \pm 180^{(7)}$
C II	1334.5323	0.1278	−0.52	0.25	-209 ± 110

(1) Absorption line; (2) Rest-frame vacuum wavelength; (3) Transition oscillator strength (see e.g., Pettini et al. 2002; Shapley et al. 2003); (4)–(5) Rest-frame EW and its 1σ ; (6) Velocity offset. (7) Values for the blended O I $\lambda 1302$ and Si II $\lambda 1304$ lines assuming that the central rest-wavelength wavelength is $\lambda = 1303.2694 \text{ Å}$.

The color excess of the stellar continuum obtained from the SED fitting is $E(B - V)_* = 0.185^{+0.009}_{-0.009}$ (CDFS-3865), $0.185^{+0.026}_{-0.018}$ (CDFS-6482), $0.273^{+0.018}_{-0.079}$ (COSMOS-13636), and $0.528^{+0.026}_{-0.026}$ (COSMOS-30679) for Calzetti et al. (2000)’s extinction law. These values are comparable to those of relatively faint (stacked) LAEs at $z \sim 2$, $E(B - V)_* = 0.27^{+0.01}_{-0.03}$ (Nakajima et al. 2012a) and $E(B - V)_* = 0.22^{+0.06}_{-0.13}$ (Guaita et al. 2011), but are larger than those of the two bright LAEs observed

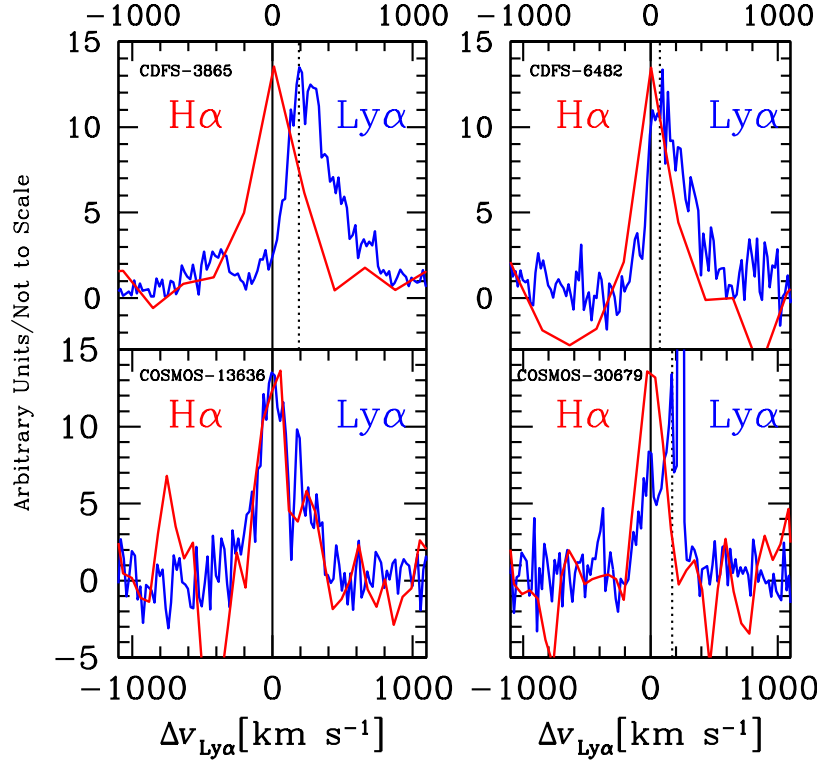


FIG. 5.— Comparison between Ly α (blue line) and H α (red line) emission profiles. The solid and dotted lines indicate the systemic and Ly α redshifts, respectively. *Top left*: CDFS-3865 with $\Delta v_{\text{Ly}\alpha} = 190^{+99}_{-18}$ km s $^{-1}$. *Top right*: CDFS-6482 with $\Delta v_{\text{Ly}\alpha} = 75^{+52}_{-25}$ km s $^{-1}$. *Bottom left*: COSMOS-13636 with $\Delta v_{\text{Ly}\alpha} = 18 \pm 16$ km s $^{-1}$. *Bottom right*: COSMOS-30679 with $\Delta v_{\text{Ly}\alpha} = 170 \pm 16$ km s $^{-1}$.

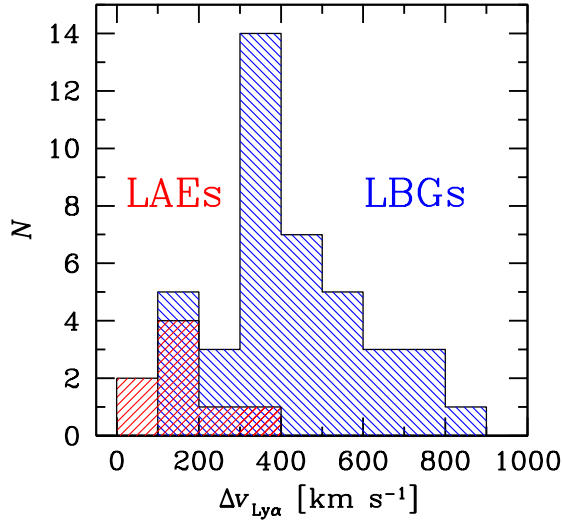


FIG. 6.— Histograms of $\Delta v_{\text{Ly}\alpha}$ for the eight LAEs studied in this paper (red) and 41 LBGs given by Steidel et al. (2010) (blue).

by Finkelstein et al. (2011), $E(B-V)_* = 0.09 \pm 0.05$ and $E(B-V)_* = 0.10 \pm 0.10$. Since our objects are as bright as Finkelstein et al. (2011)’s, this difference may indicate that LAEs at $z \sim 2$ have a wide range of dust extinction even at the same Ly α luminosity range.

Since the spectra of CDFS-3865 and CDFS-6482 cover H β as well as H α ,¹⁶ we measure the Balmer decrement (H α /H β) to constrain the color excess of nebular emission, $E(B-V)_{\text{gas}}$. The decrement values obtained are 2.96 ± 0.87 for CDFS-3865 and > 1.74 (using H β ’s 2σ limit) for CDFS-6482, which are converted into $E(B-V)_{\text{gas}} = 0.03^{+0.27}_{-0.03}$ and $E(B-V)_{\text{gas}} > 0$, respectively, adopting the intrinsic ratio of 2.86 (Osterbrock 1989) and Calzetti et al. (2000)’s extinction law.

Figure 9 plots $E(B-V)_*$ vs. $E(B-V)_{\text{gas}}$ for these objects. CDFS-3865 has $E(B-V)_{\text{gas}} \sim E(B-V)_*$. Similarly, CDFS-6482’s lower limit of $E(B-V)_{\text{gas}}$ is consistent with its $E(B-V)_*$. Thus, hereafter, we assume $E(B-V) \equiv E(B-V)_{\text{gas}} \simeq E(B-V)_*$ as proposed by Erb et al. (2006b) for starburst galaxies.

4.4. Star Formation Rate

The H α luminosity is thought to be a reliable indicator of SFR. We calculate the SFRs of our LAEs from their dust-corrected H α luminosities using Kennicutt (1998)’s formula:

$$\text{SFR}(M_{\odot} \text{ yr}^{-1}) = 7.9 \times 10^{-42} L(\text{H}\alpha) \text{ (erg s}^{-1}\text{)}, \quad (4)$$

where a Salpeter IMF is assumed. We obtain $\text{SFR} = 190 \pm 13 M_{\odot} \text{ yr}^{-1}$ (CDFS-3865), $48^{+10}_{-9} M_{\odot} \text{ yr}^{-1}$ (CDFS-6482), $17^{+3}_{-5} M_{\odot} \text{ yr}^{-1}$ (COSMOS-13636), and $45 \pm 5 M_{\odot} \text{ yr}^{-1}$ (COSMOS-30679). These values are comparable to those of Finkelstein et al. (2011)’s two LAEs,

¹⁶ COSMOS-30679 also has H β data, but the line is heavily contaminated by a sky emission line.

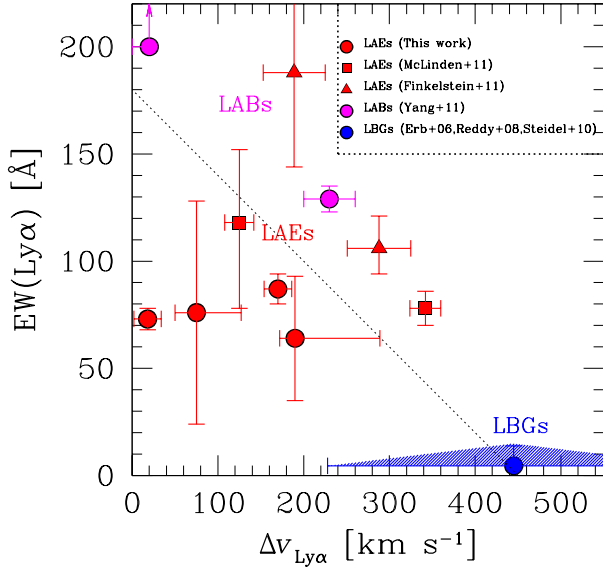


FIG. 7.— Rest-frame $\text{EW}(\text{Ly}\alpha)$ plotted against $\Delta v_{\text{Ly}\alpha}$. The red circles are our LAEs. The red square and the red triangle show the LAEs by McLinden et al. (2011) and Finkelstein et al. (2011), respectively. The blue symbol indicates the average of 41 LBGs, with the error bars corresponding to the 68 percentiles of the $\Delta v_{\text{Ly}\alpha}$ distribution (Steidel et al. 2010) and the EW distribution (Reddy et al. 2008). The magenta circles denote the LABs by Yang et al. (2011). The dotted line is the best-fit linear function to all the data points.

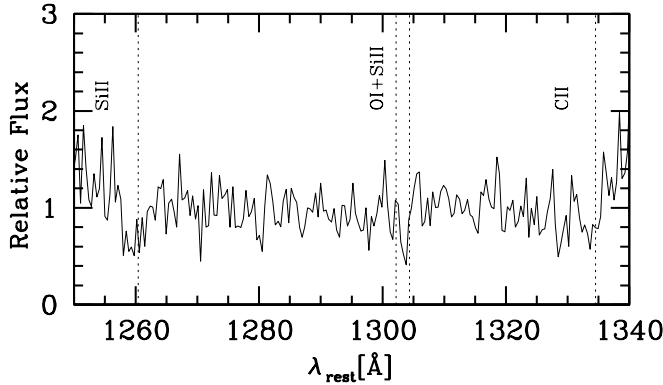


FIG. 8.— Composite FUV spectrum of the four LAEs. The spectrum has been normalized to unity in the continuum. The dotted lines indicate the rest-frame vacuum wavelengths of four LIS absorption lines. The spectrum is plotted with 0.5 \AA pix^{-1} sampling so that the profile of the blended O I and Si II lines are clearly shown.

$36.8 \pm 5.8 M_{\odot} \text{ yr}^{-1}$ and $23.6 \pm 6.5 M_{\odot} \text{ yr}^{-1}$, derived from the H α luminosity, but are larger than the average values of $z \simeq 2.2$ LAEs obtained from stacking analysis, $10 - 20 M_{\odot} \text{ yr}^{-1}$ (Nilsson et al. 2011; Nakajima et al. 2012a). This difference is reasonable, because LAEs with H α detection are generally brighter than average LAEs.

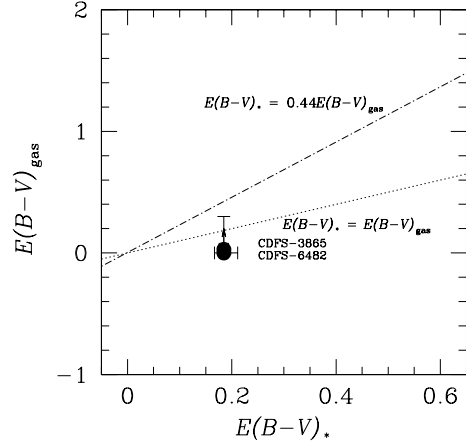


FIG. 9.— $E(B-V)_{\text{gas}}$ plotted against $E(B-V)_*$ for our two LAEs with a Balmer decrement measurement. The dotted and dashed lines correspond to $E(B-V)_* = E(B-V)_{\text{gas}}$ (Erb et al. 2006b) and $E(B-V)_* = 0.44 E(B-V)_{\text{gas}}$ (Calzetti et al. 2000), respectively.

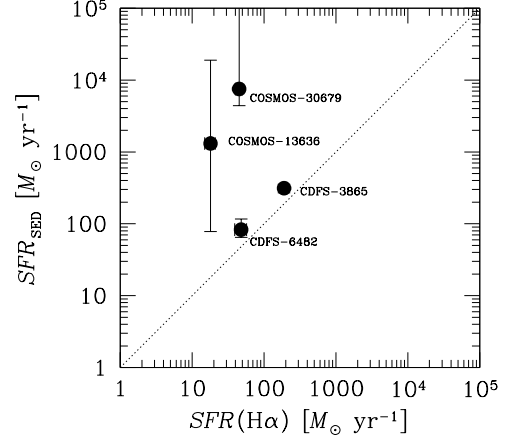


FIG. 10.— SFRs from SED fitting and from the H α luminosity. From left to right, plotted are COSMOS-13636, COSMOS-30679, CDFS-6482, and CDFS-3865.

Figure 10 plots the SFR from SED fitting against that from the H α luminosity for our objects. Although the two SFR values are comparable for CDFS-3865 and CDFS-6482, they are largely different for COSMOS-13636 and COSMOS-30679, indicating that models with very different star formation histories can fit the observed SED almost equally well. This figure thus demonstrates that it is important to measure the H α luminosity to derive a reliable SFR. In the rest of this paper, we quote the SFRs obtained from the H α luminosity.

4.5. Ly α Escape Fraction

The Ly α escape fraction of a galaxy, $f_{\text{esc}}^{\text{Ly}\alpha}$, is defined as the ratio of the observed Ly α flux to the intrinsic Ly α

flux produced in the galaxy. This quantity can be a probe of the distribution and kinematics of the ISM. For example, the outflowing ISM would make $f_{\text{esc}}^{\text{Ly}\alpha}$ larger since the number of resonant scattering and thus the chance of absorption by dust are reduced (e.g., Kunth et al. 1998; Atek et al. 2008). A clumpy distribution of the ISM would also make $f_{\text{esc}}^{\text{Ly}\alpha}$ larger (e.g., Hansen & Oh 2006; Finkelstein et al. 2008). In the clumpy ISM, HII regions where both Ly α and nebular lines originate are surrounded by clumpy gas clouds with well-mixed HI gas and dust (see, e.g., Fig. 1 of Neufeld 1990). We discuss the extent of clumpiness for our objects in §5.3.2.

Assuming the Case B recombination where the intrinsic Ly α /H α ratio is 8.7 (Brocklehurst 1971), we estimate the Ly α escape fraction as:

$$f_{\text{esc}}^{\text{Ly}\alpha} \equiv \frac{L_{\text{obs}}(\text{Ly}\alpha)}{L_{\text{int}}(\text{Ly}\alpha)} = \frac{L_{\text{obs}}(\text{Ly}\alpha)}{8.7 L_{\text{int}}(\text{H}\alpha)}, \quad (5)$$

where subscripts 'int' and 'obs' refer to intrinsic and observed quantities, respectively, and $L_{\text{int}}(\text{H}\alpha)$ is obtained by correcting the observed H α luminosity for dust extinction. We derive the $L_{\text{obs}}(\text{Ly}\alpha)$ of each object from its narrow and broad-band photometry on the assumption of a flat continuum, taking account of the exact position of the Ly α emission in the NB387 response function and applying Madau (1995)'s prescription to correct for the IGM attenuation. Note that these $f_{\text{esc}}^{\text{Ly}\alpha}$ values are not measurements but estimates, because we assume the Case B recombination.

We find $f_{\text{esc}}^{\text{Ly}\alpha} = 0.14 \pm 0.03$ (CDFs-3865), 0.29 ± 0.20 (CDFs-6482), 0.57 ± 0.13 (COSMOS-13636), and 0.17 ± 0.03 (COSMOS-30679). These values are much higher than the average value of $z \sim 2$ star-forming galaxies, $\sim 5\%$ (Hayes et al. 2010), but similar to the median value of 89 LAEs at $2 < z < 4$, $\sim 29\%$, obtained by Blanc et al. (2011). It is interesting because our LAEs have relatively large $E(B-V)$ values (Table 5). This would suggest that some mechanisms allow Ly α photons to escape from the moderately dusty ISM (Atek et al. 2008).

4.6. Size

Assuming that stars dominate the total mass of the luminous (i.e., H α emitting) part of galaxies, we infer the size of our objects from the virial theorem as:

$$r = G \frac{M_*}{\sigma_v(\text{H}\alpha)^2} \sim 4.3 \times \frac{M_*/10^{10} M_\odot}{(\sigma_v(\text{H}\alpha)/100 \text{ km s}^{-1})^2} \text{ (kpc)}, \quad (6)$$

where M_* is the stellar mass and $\sigma_v(\text{H}\alpha)$ is the velocity dispersion measured from the H α line, corrected for the instrumental velocity dispersion ($\sigma_{\text{inst.}} = 86$ [91] km s $^{-1}$ for NIRSPEC [MMIRS]). It is known that for local galaxies stellar masses dominate total masses within effective radii (see e.g., Fig 2.a in van Dokkum et al. 2009) and that for high- z galaxies total masses can be larger than stellar masses up to a factor of several (Erb et al. 2006b; van Dokkum et al. 2009). Thus, our size estimates appear to be reasonable approximations of the true values within a factor of two or so.

We obtain $r = 1.1^{+0.1}_{-0.1}$ kpc (CDFs-3865), $5.0^{+1.1}_{-0.8}$ kpc (CDFs-6482), $9.0^{+1.8}_{-4.8}$ kpc (COSMOS-13636), and $107.5^{+35.6}_{-31.6}$ kpc (COSMOS-30679). Similarly, we derive

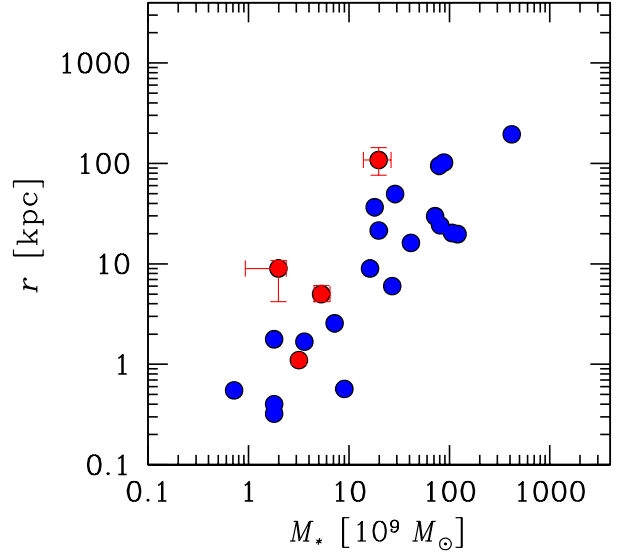


FIG. 11.— Size plotted against stellar mass. The red circles denote our LAEs, while the blue circles represent 20 LBGs which have reliable measurements of stellar mass and H α velocity dispersion (Erb et al. 2006b; Steidel et al. 2010).

sizes for 20 LBGs of Erb et al. (2006b) which have measurements of stellar mass and H α velocity dispersion. Here we multiply the stellar masses of Erb et al.'s objects by 1.8, since they assume a Chabrier IMF (Chabrier 2003). As found from Figure 11, the LAEs and LBGs roughly lie on a single size-stellar mass relation, suggesting that typical LAEs are smaller than LBGs just because they are less massive.

The physical quantities presented in this section are summarized in Table 7

5. DISCUSSION

5.1. $\Delta v_{\text{Ly}\alpha}$ and the Gas Motions of LAEs

Due to the resonant nature of Ly α , the observed Ly α line of a galaxy has a complicated profile depending on the kinematics and geometry of the ISM. A Ly α source in a simple static gas cloud produces a symmetric double-peaked profile centered at 1216 Å due to significant resonant scattering at 1216 Å (Harrington 1973; Neufeld 1990; Dijkstra et al. 2006). If the bluer peak is heavily absorbed by the intervening IGM along the line of sight, only the redder peak will be observed. In the case of outflow, the Ly α emission line should show an asymmetric profile similar to a P Cygni profile. Verhamme et al. (2006) have explained some of observed Ly α profiles with a strong red peak and a weak blue peak with models of an expanding shell that absorbs Ly α photons at around 1216 Å, although the surface brightness distribution may not be explained by such wind shells (see, e.g., Barnes & Haehnelt 2009). In short, when an outflow exists, the observed Ly α line should show an asymmetric profile with a strong peak redshifted with respect to the systemic velocity.

We measure the offset velocity of the Ly α peak,

$\Delta v_{\text{Ly}\alpha}$, in §4.1. To quantify the asymmetry of the Ly α line of our objects, we use the weighted skewness, S_w (Kashikawa et al. 2006). Skewness is the third moment of the flux distribution, and the weighted skewness is defined as the product of the skewness and the line width. A positive S_w means that the Ly α profile has a red tail as in the case of outflow. We obtain $S_w = 6.03 \pm 0.51$ (CDFS-3865), 5.45 ± 1.59 (CDFS-6482), 1.01 ± 0.76 (COSMOS-13636), and 5.31 ± 4.06 (COSMOS-30679)¹⁷.

As found in §4.1, three out of the four objects have a positive $\Delta v_{\text{Ly}\alpha}$ beyond the 2σ uncertainty. This result, combined with the positive measurements of S_w , leads us to a conclusion that the Ly α emission of our objects is mostly originated from outflowing gas. This conclusion is supported by the fact obtained in §4.2 that the LIS absorption lines of the composite spectrum are blue-shifted with respect to the systemic velocity.

Using simulations of Ly α radiative transfer in outflowing galaxies, Verhamme et al. (2006, 2008) suggest that not only LIS absorption lines but also the Ly α line can be used to estimate the outflow velocity. Their simulations assume that a galaxy is surrounded by a spherically symmetric shell-like outflowing gas cloud in which H I gas and dust are well mixed. They find that for relatively low H I column densities of $N_{\text{H}} \lesssim 10^{20} \text{ cm}^{-2}$, the peak of the Ly α profile emerges near the outflow velocity, giving $\Delta v_{\text{Ly}\alpha} \sim v_{\text{out}}$, while for high column densities of $N_{\text{H}} \gtrsim 10^{20} \text{ cm}^{-2}$, the peak is offset twice the outflow velocity, giving $\Delta v_{\text{Ly}\alpha} \approx 2v_{\text{out}}$. In any case, it is suggested that $\Delta v_{\text{Ly}\alpha}$ positively correlates with v_{out} .

On a reasonable assumption that $\Delta v_{\text{Ly}\alpha}$ positively correlates with the speed of an outflow within a factor of 2, one can test the hypothesis that Ly α photons can escape more easily for a larger outflow velocity, due to the reduced number of resonant scattering (e.g., Kunth et al. 1998). If this is the case, we should find a positive correlation between $\Delta v_{\text{Ly}\alpha}$ and EW(Ly α). However, Figure 7 indicates an opposite tendency. Furthermore, we find in §4.2 that LAEs and LBGs have similar average Δv_{abs} , i.e., similar average outflow velocities. These two findings would suggest that outflows are not the physical origin of large-EW(Ly α) objects.

In §4.1, we find that the average $\Delta v_{\text{Ly}\alpha}$ of LAEs is $175 \pm 35 \text{ km s}^{-1}$, which is significantly smaller than that of LBGs ($\simeq 400 \text{ km s}^{-1}$) at similar redshifts. This result is important not only for understanding the physical origin of Ly α emission in galaxies, but also for probing cosmic reionization with LAEs. If LAEs at $z > 6$ have similarly small $\Delta v_{\text{Ly}\alpha}$ values, the amount of Ly α photons scattered by the IGM, as used to constrain the epoch of reionization, may be in need of revision. For example, Santos (2004) has examined the transmission through the IGM of Ly α photons emitted from a galaxy for two cases, $\Delta v_{\text{Ly}\alpha} = 0$ and 360 km s^{-1} , the latter of which is comparable to the average $\Delta v_{\text{Ly}\alpha}$ of $z \sim 2 - 3$ LBGs. Some recent reionization studies using LAEs assume the latter case to estimate the neutral hydrogen fraction of the IGM, x_{HI} , at $z > 6$ (e.g., Kashikawa et al. 2006; Ota et al. 2008; Ouchi et al. 2010; Kashikawa et al. 2011). However, if $z > 6$ LAEs have $\Delta v_{\text{Ly}\alpha}$ as small as

$\simeq 175 \text{ km s}^{-1}$, these studies may be overestimating x_{HI} . Similarly, Ono et al. (2012), Schenker et al. (2012), and Pentericci et al. (2011) have derived x_{HI} as large as $\sim 40 - 60\%$ from a significant drop in the fraction of large-EW(Ly α) galaxies from $z \sim 6$ to 7. If such a high value were correct, reionization would take place very late, which cannot easily be reconciled with constraints from the Lyman alpha forest opacity (Becker et al. 2007) or the large value of the Thomson optical depth, $\tau = 0.09$, obtained by WMAP observations (Dunkley et al. 2009; Komatsu et al. 2011). Future Ly α emission models for reionization studies would need to use our result of a small average $\Delta v_{\text{Ly}\alpha}$ value if $\Delta v_{\text{Ly}\alpha}$ does not significantly evolve over cosmic time.

5.2. Correlations Between Outflow Velocity and Physical Properties

5.2.1. Outflow Velocity and SFR

We first examine the correlation between $\Delta v_{\text{Ly}\alpha}$, which represents the outflow velocity within a factor of two as discussed in §5.1, and the SFR for LAEs and LBGs. For the present-day universe, Martin (2005) has found in a sample of ULIRGs, LIRGs, and starburst dwarfs that those with a larger outflow velocity tend to have a higher SFR, roughly following a power-law of $v_{\text{out}} \propto \text{SFR}^{0.35}$. Note that this sample spans four orders of magnitude in the SFR. This correlation implies that galaxies with a high SFR tend to have more massive stars and SNe which drive outflows. As pointed out by some authors (e.g., Martin 2005; Steidel et al. 2010), the correlation flattens and is difficult to see for objects with intermediate SFRs of $10 - 100 M_{\odot} \text{ yr}^{-1}$.

From the left panel of Figure 12, there may exist a positive correlation between $\Delta v_{\text{Ly}\alpha}$ and SFR for LAEs, which is roughly consistent with $\Delta v_{\text{Ly}\alpha} \propto \text{SFR}$, although the statistics is not very good. For LBGs, which are taken from the literature (Erb et al. 2006b; Steidel et al. 2010), a much flatter correlation is seen. Thus, it is found that LAEs and LBGs do not follow the same power law, and that LAEs have comparable to or systematically smaller outflow velocities at a given SFR, even when we take account of the possibility that $\Delta v_{\text{Ly}\alpha}$ may overestimate v_{out} up to a factor two. Theoretically, the slope of the correlation depends on the dominant physical outflow process (Kornei et al. 2012). A linear correlation, $v_{\text{out}} \propto \text{SFR}$, is expected for radiation pressure dominant outflows (Sharma et al. 2011), while shallower slopes are indicative of ram pressure dominant outflows (Heckman et al. 2000). It appears that outflows in LAEs are at least consistent with the radiation pressure case.

5.2.2. Outflow Velocity and $\sigma_v(\text{H}\alpha)$

We then examine how $\Delta v_{\text{Ly}\alpha}$ correlates with $\sigma_v(\text{H}\alpha)$, which is related to the gravitational potential of galaxies. Martin (2005) has found that the terminal outflow velocity always approaches the galactic escape velocity, which is consistent with a theoretical prediction (e.g., Murray et al. 2005). The middle panel of Figure 12 presents $\Delta v_{\text{Ly}\alpha}$ as a function of $\sigma_v(\text{H}\alpha)$ for our LAEs, together with those of ~ 20 LBGs (Erb et al. 2006b; Steidel et al. 2010). It is not clear whether there exists a correlation with the given poor statistics and large errors. However, LAEs are found to have comparable to or smaller outflow velocities than LBGs at a given $\sigma_v(\text{H}\alpha)$.

¹⁷ The S_w of COSMOS-30679 is calculated after masking the wavelength range affected by the cosmic ray.

5.2.3. Outflow Velocity and SFR Surface Density

Finally, we examine the correlation with the SFR surface density, Σ_{SFR} , which represents the intensity of star forming activity. The right panel of Figure 12 plots $\Delta v_{\text{Ly}\alpha}$ against Σ_{SFR} for our LAEs and LBGs taken from the literature. Here we estimate Σ_{SFR} by dividing the SFR by πr^2 , where r is the size derived in §4.6. The Σ_{SFR} values of our objects are $157^{+31}_{-31} M_{\odot} \text{ yr}^{-1} \text{ kpc}^{-2}$ (CDFS-3865), $1.9^{+0.9}_{-0.7} M_{\odot} \text{ yr}^{-1} \text{ kpc}^{-2}$ (CDFS-6482), $0.22^{+0.096}_{-0.22} M_{\odot} \text{ yr}^{-1} \text{ kpc}^{-2}$ (COSMOS-13636), and $3.89^{+2.62}_{-2.33} \times 10^{-3} M_{\odot} \text{ yr}^{-1} \text{ kpc}^{-2}$ (COSMOS-30679).¹⁸ Again, LAEs are found to have comparable to or smaller outflow velocities than LBGs at a given Σ_{SFR} .

To summarize, we find that LAEs tend to have comparable to or smaller outflow velocities than LBGs and that LAEs and LBGs have different slopes of the $\Delta v_{\text{Ly}\alpha}$ -SFR relation. These findings imply that the physical origin of LAEs' outflows appears to be different from that of LBGs'.

5.3. Why LAEs Have Strong Ly α Emission?

In this subsection, we discuss the physical origin of strong Ly α emission from LAEs. There are various mechanisms capable of enhancing Ly α emission: shock heating by an inflow or outflow, very weak dust extinction, a peculiar geometry of dust/gas clouds, a low neutral hydrogen column density, and a high outflow velocity. The high outflow velocity hypothesis is found to be unlikely in §5.1 (see also the left panels of Figure 13). Here we examine the weak-dust extinction hypothesis, clumpy-cloud hypothesis, and low- N_{H} hypothesis.

5.3.1. Weak Dust Extinction

It is possible that Ly α photons survive through resonant scattering in gas clouds with little dust. In this case, one should find significantly small $E(B-V)$ in LAEs and a negative correlation between $E(B-V)$ and $\text{EW}(\text{Ly}\alpha)$. The middle panels of Figure 13 plot $\text{EW}(\text{Ly}\alpha)$ and $f_{\text{esc}}^{\text{Ly}\alpha}$ as functions of $E(B-V)$. There is no significant correlation in either panel. Hayes et al. (2010) and Kornei et al. (2010) have reported an anti-correlation between $f_{\text{esc}}^{\text{Ly}\alpha}$ and $E(B-V)$ in H α emitters at $z \simeq 2.2$ and LBGs at $z \sim 3$, respectively. However, in our $f_{\text{esc}}^{\text{Ly}\alpha}$ vs $E(B-V)$ plot, there are objects with relatively high $f_{\text{esc}}^{\text{Ly}\alpha}$ of 0.3–0.6 even in a moderately high extinction of $E(B-V) = 0.2$ –0.3. Therefore, it is not clear if weak dust extinction solely can explain the strong Ly α emission.

5.3.2. Clumpy Clouds

The gas distribution in LAEs may not be smooth and spherically symmetric, but clumpy. In a clumpy geometry, dust grains are shielded by H I gas, and Ly α photons are resonantly scattered on the surfaces of clouds without being absorbed by dust (Neufeld 1991; Hansen & Oh 2006). Because continuum photons are absorbed through dusty gas clouds, the ratio of Ly α to UV continuum

fluxes, or $\text{EW}(\text{Ly}\alpha)$, is enhanced. For a further discussion of the clumpy-cloud hypothesis, we calculate the clumpiness parameter, q , introduced by Finkelstein et al. (2008):

$$q = \tau(\text{Ly}\alpha) / \tau_{1216}, \quad (7)$$

where $\tau(\text{Ly}\alpha)$ and τ_{1216} are defined as $e^{-\tau(\text{Ly}\alpha)} = L_{\text{obs}}(\text{Ly}\alpha) / L_{\text{int}}(\text{Ly}\alpha)$ and $e^{-\tau_{1216}} = 10^{-0.4k_{1216}E(B-V)}$ with the extinction coefficient at $\lambda = 1216 \text{ \AA}$, $k_{1216} = 11.98$ (Calzetti et al. 2000). This parameter is used to diagnose the geometry of the ISM (e.g., Finkelstein et al. 2008; Kornei et al. 2010; Nakajima et al. 2012a). If the geometry of the ISM is clumpy, q is smaller than unity. In the case of $q > 1$, Ly α photons are more preferentially absorbed by dust through the relatively homogeneous ISM.

The q values of our objects are calculated to be $q = 0.96 \pm 0.11$ (CDFS-3865), 0.61 ± 0.34 (CDFS-6482), $0.19^{+0.07}_{-0.09}$ (COSMOS-13636), and $0.30^{+0.03}_{-0.03}$ (COSMOS-30679); three out of the four clearly have $q < 1$ beyond the uncertainties. These results are consistent with that of Nakajima et al. (2012a) who obtained $q = 0.7^{+0.1}_{-0.1}$ for $z \simeq 2.2$ stacked LAEs. On the other hand, some studies have found more LAEs with $q > 1$ at $z \sim 2$ (e.g., Nilsson et al. 2009; Hayes et al. 2010).

The right panels of Figure 13 show $f_{\text{esc}}^{\text{Ly}\alpha}$ and $\text{EW}(\text{Ly}\alpha)$ as functions of q for the LAE sample. There may exist a negative correlation between q and $f_{\text{esc}}^{\text{Ly}\alpha}$, although not very clear due to the poor statistics.

5.3.3. Low N_{H}

Finally, we examine the possibility that the N_{H} of LAEs is relatively low. To constrain N_{H} for LAEs and LBGs, we use the dependence of $\Delta v_{\text{Ly}\alpha}$ on N_{H} found by Verhamme et al. (2006, 2008). As mentioned in §5.1, they find $\Delta v_{\text{Ly}\alpha} \approx 2v_{\text{out}}$ for $N_{\text{H}} \gtrsim 10^{20} \text{ cm}^{-2}$ while $\Delta v_{\text{Ly}\alpha} \sim v_{\text{out}}$ for $N_{\text{H}} \lesssim 10^{20} \text{ cm}^{-2}$; $\Delta v_{\text{Ly}\alpha}$ is smaller for lower N_{H} due to a smaller amount of wavelength shift by resonant scattering. Since $|\Delta v_{\text{abs}}|$ is equal to v_{out} in an expanding shell, one can thus use $\Delta v_{\text{Ly}\alpha}$ and Δv_{abs} to distinguish between high and low H I column densities.

The LAEs we study have average velocities of $\Delta v_{\text{Ly}\alpha} = 175 \pm 35 \text{ km s}^{-1}$ and $\Delta v_{\text{abs}} = -179 \pm 73 \text{ km s}^{-1}$, i.e., $\Delta v_{\text{Ly}\alpha} \approx |\Delta v_{\text{abs}}|$, while LBGs have $\Delta v_{\text{Ly}\alpha} \approx 2$ – $3 \times |\Delta v_{\text{abs}}|$ (Steidel et al. 2010; Rakic et al. 2011). This suggests that LAEs have on average lower N_{H} than LBGs.

For a lower N_{H} , Ly α photons have a reduced chance of absorption by dust before escaping the galaxy because of a smaller number of resonant scattering. Thus, we infer that LAEs have strong Ly α emission because of low H I column densities. Although our data tell nothing about why LAEs have low column densities, possible reasons would include a high gas temperature caused by a shock heating (Nakajima et al. 2012b), which reduces the fraction of neutral hydrogen, and a clumpy gas geometry (Bond et al. 2010).

¹⁸ Although many studies have adopted Petrosian radius for the size of a galaxy, it is known that Petrosian radius is likely to overestimate the area of the star forming region of galaxies especially for high- z objects with a clumpy star forming region (Kornei et al. 2012).

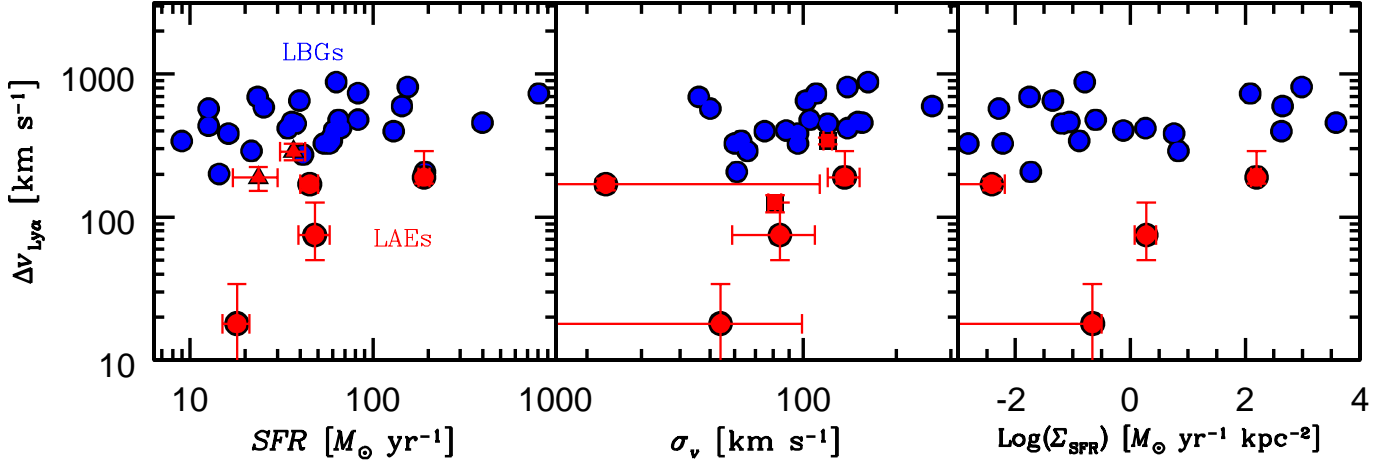


FIG. 12.— $\Delta v_{\text{Ly}\alpha}$ as a function of SFR (left panel), $\sigma_v(\text{H}\alpha)$ (middle), and Σ_{SFR} (right). For all panels, the red and blue circles indicate, respectively, our LAEs and LBGs taken from the literature. The red triangles in the left panel denote LAEs at $z \sim 2.3$ (Finkelstein et al. 2011), and the red squares in the middle panel indicate LAEs at $z \sim 3$ (McLinden et al. 2011).

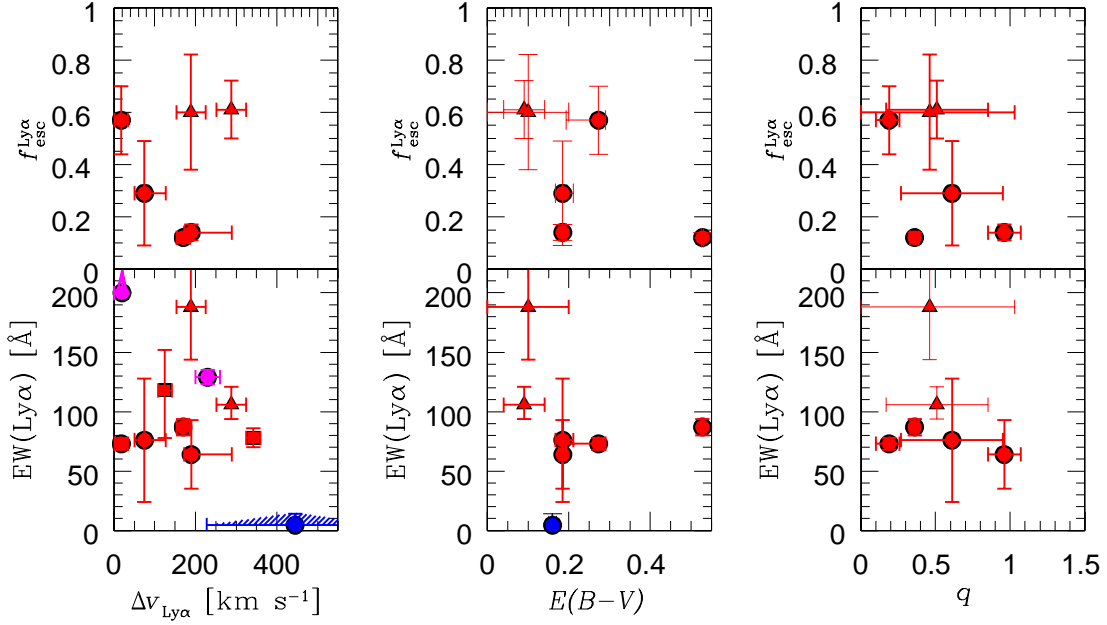


FIG. 13.— $f_{\text{esc}}^{\text{Ly}\alpha}$ and $\text{EW}(\text{Ly}\alpha)$ plotted against $\Delta v_{\text{Ly}\alpha}$, $E(B-V)$, and q . The red circles denote our LAEs. The red squares and triangles are the LAEs given by McLinden et al. (2011) and Finkelstein et al. (2011), respectively. The magenta circles and blue circles represent, respectively, LABs (Yang et al. 2011) and LBGs (Erb et al. 2006b; Reddy et al. 2008; Steidel et al. 2010).

TABLE 7
SUMMARY OF THE PHYSICAL QUANTITIES

Object	$E(B-V)_*$	M_* $10^9 M_{\odot}$	$\text{EW}(\text{Ly}\alpha)$ Å	$\Delta v_{\text{Ly}\alpha}$ km s $^{-1}$	$L(\text{H}\alpha)$ $10^{41} \text{ erg s}^{-1}$	$\sigma_v(\text{H}\alpha)$ km s $^{-1}$	$SFR(\text{H}\alpha)$ $M_{\odot} \text{ yr}^{-1}$	$f_{\text{esc}}^{\text{Ly}\alpha}$	r kpc	q
	(1)	(2)	(3)	(4)	(5)	(6)	(7)	(8)	(9)	(10)
CDFS-3865	$0.185^{+0.009}_{-0.009}$	$3.18^{+0.21}_{-0.13}$	64^{+29}_{-29}	190^{+99}_{-18}	$136.5^{+8.5}_{-8.5}$	110.8	190^{+13}_{-13}	$0.14^{+0.03}_{-0.03}$	$1.1^{+0.1}_{-0.1}$	$0.96^{+0.11}_{-0.11}$
CDFS-6482	$0.185^{+0.026}_{-0.018}$	$5.30^{+1.18}_{-0.80}$	76^{+52}_{-52}	75^{+52}_{-25}	$34.5^{+6.2}_{-6.2}$	67.5	48^{+10}_{-9}	$0.29^{+0.20}_{-0.20}$	$5.0^{+1.1}_{-0.8}$	$0.61^{+0.34}_{-0.34}$
COSMOS-13636	$0.273^{+0.039}_{-0.079}$	$1.99^{+0.39}_{-1.06}$	73^{+5}_{-5}	18^{+16}_{-16}	$9.5^{+1.3}_{-1.3}$	30.7	18^{+3}_{-3}	$0.57^{+0.13}_{-0.13}$	$9.0^{+1.8}_{-4.8}$	$0.19^{+0.07}_{-0.09}$
COSMOS-30679	$0.528^{+0.0026}_{-0.0026}$	$19.75^{+6.53}_{-5.80}$	87^{+7}_{-7}	170^{+16}_{-16}	$11.4^{+1.0}_{-1.0}$	28.1	45^{+5}_{-5}	$0.17^{+0.03}_{-0.03}$	$107.5^{+35.6}_{-31.6}$	$0.30^{+0.03}_{-0.03}$

Notes. (1) Dust extinction estimated from SED fitting; (2) Stellar mass estimated from SED fitting; (3) Rest-frame Ly α EW; (4) Velocity offset of the Ly α line; (5) H α luminosity; (6) Velocity dispersion of H α line; (7) Star formation rate from H α luminosity corrected for dust extinction; (8) Ly α escape fraction estimated in §4.5; (9) Size of the galaxy derived in §4.6 under the assumption that stars dominate the total mass in the luminous part of the galaxy; (10) Clumpiness parameter (§5.3.2).

We have presented the results of Magellan/MMIRS and Keck/NIRSPEC spectroscopy for five LAEs at $z \simeq 2.2$ for which high-resolution FUV spectra from Magellan/MagE are available. These objects are taken from the $z \simeq 2.2$ LAE samples constructed by K. Nakajima et al. (in preparation: see Nakajima et al. 2012a for the selection). The redshift of $z \simeq 2.2$ is unique since we can observe from the ground all of Ly α , LIS absorption lines, and optical nebular emission lines including H α .

We have successfully detected H α emission from all five objects, and [OII] $\lambda\lambda 3726, 3729$, H β , and/or [OIII] $\lambda\lambda 4959, 5007$ for some LAEs on the individual basis. In addition to that, we have detected LIS absorption lines in a stacked FUV spectrum. After removing an AGN-contaminated object, we have measured the velocity offsets of the Ly α line ($\Delta v_{\text{Ly}\alpha}$) and of LIS absorption lines (Δv_{abs}) from the systemic redshift determined by nebular emission lines, to discuss the gas motions of LAEs. The major results of our study are summarized below.

- We have obtained $\Delta v_{\text{Ly}\alpha} = 190^{+99}_{-18} \text{ km s}^{-1}$ (CDFS-3865), $75^{+52}_{-25} \text{ km s}^{-1}$ (CDFS-6482), $18 \pm 16 \text{ km s}^{-1}$ (COSMOS-13636), and $170 \pm 16 \text{ km s}^{-1}$ (COSMOS-30679); three out of the four have a positive $\Delta v_{\text{Ly}\alpha}$ beyond the 2σ uncertainty. Combining with the result that all four have a positive weighted skewness, we have conclude that the Ly α emission of our objects is mostly originated from outflowing gas. This conclusion is supported by the finding that the LIS absorption lines in the stacked FUV spectrum are blue-shifted with $\Delta v_{\text{abs}} = -179 \pm 73 \text{ km s}^{-1}$.
- For a sample of eight $z \sim 2\text{--}3$ LAEs without AGN from our study and the literature, we have obtained $\Delta v_{\text{Ly}\alpha} = 175 \pm 35 \text{ km s}^{-1}$, which is significantly smaller than that of LBGs, $\Delta v_{\text{Ly}\alpha} \simeq 400 \text{ km s}^{-1}$. If LAEs at $z > 6$ have similarly small $\Delta v_{\text{Ly}\alpha}$ values, some reionization studies based on LAEs assuming $\Delta v_{\text{Ly}\alpha}$ as large as that of LBGs may be overestimating the neutral fraction of the IGM.
- We have found an anti-correlation between EW(Ly α) and $\Delta v_{\text{Ly}\alpha}$ in a compilation of LAE, LAB, and LBG samples, i.e., EW(Ly α) decreases with $\Delta v_{\text{Ly}\alpha}$. On a reasonable assumption that $\Delta v_{\text{Ly}\alpha}$ positively correlates with the outflow velocity within a factor of two, this anti-correlation indicates that high outflow velocities are not the physical origin of the strong Ly α emission of LAEs.
- We have found that LAEs have comparable to or

smaller outflow velocities than LBGs at a given SFR , $\sigma(\text{H}\alpha)$, and Σ_{SFR} (when the systematic error of $\lesssim 2$ in $\Delta v_{\text{Ly}\alpha}$ as a measure of v_{out} is considered). We have also found that the slope of the $\Delta v_{\text{Ly}\alpha}$ - SFR relation is different between LAEs and LBGs. Thus, the physical origin of LAEs' outflows appears to be different from that of LBGs'. It appears that LAEs' outflows are at least consistent with the radiation pressure case.

- To identify the physical origin of large-EW(Ly α) galaxies, we have tested three hypotheses which may facilitate the escape of Ly α photons: weak dust extinction, clumpy-cloud geometry, and low N_{H} . Since we have found no significant correlation between EW(Ly α) and $E(B - V)$, it is not clear if weak dust extinction leads to a high escape fraction of Ly α photons. Although there may exist an anti-correlation between $f_{\text{esc}}^{\text{Ly}\alpha}$ and the clumpiness parameter, more data and theoretical work are needed to draw a firm conclusion.
- We have found that LAEs have $\Delta v_{\text{Ly}\alpha} \approx |\Delta v_{\text{abs}}|$, in contrast with LBGs which have $\Delta v_{\text{Ly}\alpha} \approx 2\text{--}3 \times |\Delta v_{\text{abs}}|$. When combined with the simulations of Ly α radiative transfer in a galaxy with an expanding shell of the ISM by Verhamme et al. 2006, 2008, this suggests that the typical N_{H} of LAEs would be lower than that of LBGs, giving a smaller number of resonant scattering. Such low N_{H} may cause the observed strong Ly α emission of LAEs.

ACKNOWLEDGEMENTS

We thank an anonymous referee for valuable comments that have greatly improved the paper. We are grateful to Kentaro Motohara and Masakazu Kobayashi for their helpful comments. We acknowledge Brian McLeod and Paul Martini who gave us helpful advice on our MMIRS observations and data reduction. We are deeply grateful to Magellan and Keck Telescope staff for supporting our MMIRS and NIRSPEC observations. We also thank Yujin Yang for providing photometry data of two LABs, Steven Finkelstein for providing the revised results of his work, Daniel Stark, Ann Zabludoff, Masayuki Umemura, Hannes Jensen, and Matthew Schenker for giving us various useful comments. This work was supported by KAKENHI (23244025) Grant-in-Aid for Scientific Research(A) through Japan Society for the Promotion of Science (JSPS), and NSF grant 1108815 awarded by National Science Foundation.

REFERENCES

- Atek, H., Kunth, D., Hayes, M., Östlin, G., & Mas-Hesse, L. M. 2008, *A&A*, 488, 491
- Baldwin, J. A., Phillips, M. M., & Terlevich, R. 1981, *PASP*, 93, 5
- Barnes, L. A. and Haehnelt, M. G. 2009, *MNRAS*, 397, 511
- Becker, G. D., Rauch, M., & Sargent, W. L. W. 2007, *ApJ*, 662, 72
- Blanc, G. A., et al. 2011, *ApJ*, 736, 31
- Bond, N. A., Gawiser, E., Gronwall, C., Ciardullo, R., Altmann, M., & Schawinski, K. 2009, *ApJ*, 705, 639
- Bond, N. A., Feldmeier, J. J., Matković, A., Gronwall, C., Ciardullo, R., & Gawiser, E. 2010, *ApJ*, 716, L200
- Brocklehurst, M. 1971, *MNRAS*, 153, 471
- Bruzual, G., & Charlot, S. 2003, *MNRAS*, 344, 1000
- Calzetti, D., Armus, L., Bohlin, R. C., Kinney, A. L., Koornneef, J., & Storchi-Bergmann, T. 2000, *ApJ*, 533, 682
- Cardamone, C. N., et al. 2010, *ApJS*, 189, 270
- Chabrier, G. 2003, *PASP*, 115, 763
- Choi, J.-H. & Nagamine, K. 2011, *MNRAS*, 410, 2579
- Cowie, L. L., Barger, A. J., & Hu, E. M. 2011, *ApJ*, 738, 136
- Daddi, E., Cimatti, A., Renzini, A., Fontana, A., Mignoli, M., Pozzetti, L., Tozzi, P., & Zamorani, G. 2004, *ApJ*, 617, 746
- Dekel, A. et al. 2009, *Nature*, 457, 451

- Dijkstra, M., Haiman, Z., & Spaans, M. 2006, *ApJ*, 649, 14
- Dunkley, J., et al. 2009, *ApJS*, 180, 306
- Elvis, M. et al. 2009, *ApJS*, 184, 158
- Erb, D. K., Shapley, A. E., Pettini, M., Steidel, C. C., Reddy, N. A., & Adelberger, K. L. 2006a, *ApJ*, 644, 813
- Erb, D. K., Steidel, C. C., Shapley, A. E., Pettini, M., Reddy, N. A., & Adelberger, K. L. 2006b, *ApJ*, 646, 107
- Finkelstein, S. L., Rhoads, J. E., Malhotra, S., Grogan, N., & Wang, J. 2008, *ApJ*, 678, 655
- Finkelstein, S. L., Papovich, C., Rudnick, G., Egami, E., Le Floch, E., Rieke, M. J., Rigby, J. R., & Willmer, C. N. A. 2009, *ApJ*, 700, 376
- Finkelstein, S. L., et al. 2011, *ApJ*, 729, 140
- Guaity, L., et al. 2011, *ApJ*, 733, 114
- Hansen, M., & Oh, S. P. 2006, *MNRAS*, 367, 979
- Harrington, J. P. 1973, *MNRAS*, 162, 43
- Hayes, M., et al. 2010, *Nature*, 464, 562
- Heckman, T. M., Armus, L., & Miley, G. K. 1990, *ApJS*, 74, 833
- Heckman, T. M., Lehnert, M. D., Strickland, D. K., & Armus, L. 2000, *ApJS*, 129, 493
- Kashikawa, N., et al. 2006, *ApJ*, 648, 7
- Kashikawa, N., et al. 2011, *ApJ*, 734, 119
- Kauffmann, G., et al. 2003, *MNRAS*, 346, 1055
- Kelson, D. D. 2003, *PASP*, 115, 688
- Kennicutt, R. C., Jr. 1998, *ARA&A*, 36, 189
- Kewley, L. J., Dopita, M. A., Sutherland, R. S., Heisler, C. A., & Trevena, J. 2001, *ApJ*, 556, 121
- Kewley, L. J., & Dopita, M. A. 2002, *ApJS*, 142, 35
- Komatsu, E., et al. 2011, *ApJS*, 192, 18
- Kornei, K. A., Shapley, A. E., Erb, D. K., Steidel, C. C., Reddy, N. A., Pettini, M., & Bogosavljević, M. 2010, *ApJ*, 711, 693
- Kornei, K. A., Shapley, A. E., Martin, C. L., Coil, A. L., Lotz, J. M., Schiminovich, D., Bundy, K. & Noeske, K. G. 2012, *ApJ*, 758, 135
- Kunth, D., Mas-Hesse, J. M., Terlevich, E., Terlevich, R., Lequeux, J., & Fall, S. M. 1998, *A&A*, 334, 11
- Larson, R. B. 1974, *MNRAS*, 169, 229
- Luo, B., et al. 2008, *ApJS*, 179, 19
- Madau, P. 1995, *ApJ*, 441, 18
- Martin, C. L. 2005, *ApJ*, 621, 227
- Matsuda, Y., et al. 2004, *AJ*, 128, 569
- McCracken, H. J., et al. 2010, *ApJ*, 708, 202
- McLinden, E. M., et al. 2011, *ApJ*, 730, 136
- Murray, N., Quataert, E., & Thompson, T. A. 2005, *ApJ*, 618, 569
- Nakajima, K., et al. 2012a, *ApJ*, 745, 12
- Nakajima, K., Ouchi, M., Shimasaku, K., Hashimoto, T., Ono, Y., & Lee, J. C. 2012b, *ArXiv e-prints*
- Neufeld, D. A. 1990, *ApJ*, 350, 216
- Neufeld, D. A. 1991, *ApJ*, 370, L85
- Nilsson, K. K., et al. 2007, *A&A*, 471, 71
- Nilsson, K. K., Tapken, C., Møller, P., Freudling, W., Fynbo, J. P. U., Meisenheimer, K., Laursen, P., & Östlin, G., 2009, *A&A*, 498, 13
- Nilsson, K. K., Östlin, G., Møller, P., Möller-Nilsson, O., Tapken, C., Freudling, W., & Fynbo, J. P. U. 2011, *A&A*, 529, A9
- Oke, J. B., & Gunn, J. E. 1983, *ApJ*, 266, 713
- Ono, Y., Ouchi, M., Shimasaku, K., Dunlop, J., Farrah, D., McLure, R., & Okamura, S. 2010a, *ApJ*, 724, 1524
- Ono, Y., et al. 2010b, *MNRAS*, 402, 1580
- Ono, Y., et al. 2012, *ApJ*, 744, 83
- Osterbrock, D. E. 1989, *Astrophysics of Gaseous Nebulae and Active Galactic Nuclei*. University Science Books, Sausalito, CA
- Ota, K., et al. 2008, *ApJ*, 677, 12
- Ouchi, M., et al. 2010, *ApJ*, 723, 869
- Peng, C. Y., Ho, L. C., Impey, C. D., & Rix, H.-W. 2002, *AJ*, 124, 266
- Pentericci, L., et al. 2011, *ApJ*, 743, 132
- Pettini, M., Rix, S. A., Steidel, C. C., Adelberger, K. L., Hunt, M. P., & Shapley, A. E. 2002, *ApJ*, 569, 742
- Rakic, O., Schaye, J., Steidel, C. C., & Rudie, G. C. 2011, *MNRAS*, 414, 3265
- Rauch, M., et al. 2008, *ApJ*, 681, 856
- Reddy, N. A., Steidel, C. C., Pettini, M., Adelberger, K. L., Shapley, A. E., Erb, D. K., & Dickinson, M. 2008, *ApJS*, 175, 48
- Salpeter, E. E. 1955, *ApJ*, 121, 161
- Santos, M. R. 2004, *MNRAS*, 349, 1137
- Schaerer, D., & de Barros, S. 2009, *A&A*, 502, 423
- Schenker, M. A., Stark, D. P., Ellis, R. S., Robertson, B. E., Dunlop, J. S., McLure, R. J., Kneib, J.-P., & Richard, J. 2012, *ApJ*, 744, 179
- Schinnerer, E., et al. 2010, *ApJS*, 188, 384
- Shapley, A. E., Steidel, C. C., Pettini, M., & Adelberger, K. L. 2003, *ApJ*, 588, 65
- Shapley, A. E., Erb, D. K., Pettini, M., Steidel, C. C., & Adelberger, K. L. 2004, *ApJ*, 612, 108
- Sharma, M., Nath, B. B., & Shchekinov, Y. 2011, *ApJ*, 736, L27
- Steidel, C. C., Adelberger, K. L., Shapley, A. E., Pettini, M., Dickinson, M., & Giavalisco, M. 2000, *ApJ*, 532, 170
- Steidel, C. C., Erb, D. K., Shapley, A. E., Pettini, M., Reddy, N., Bogosavljević, M., Rudie, G. C., & Rakic, O. 2010, *ApJ*, 717, 289
- Tremonti, C. A., et al. 2004, *ApJ*, 613, 898
- van Dokkum P. G., Kriek M., Franx M. 2009, *Nat*, 460, 717
- Verhamme, A., Schaerer, D., Atek, H., & Tapken, C. 2008, *A&A*, 491, 89
- Verhamme, A., Schaerer, D., & Maselli, A. 2006, *A&A*, 460, 397
- Yang, Y., Zabludoff, A., Tremonti, C., Eisenstein, D., & Davé, R. 2009, *ApJ*, 693, 1579
- Yang, Y., Zabludoff, A., Jahnke, K., Eisenstein, D., Davé, R., Shectman, S. A., & Kelson, D. D. 2011, *ApJ*, 735, 87
- Yuma, S., Ohta, K., & Yabe, K. 2012, *ArXiv e-prints*